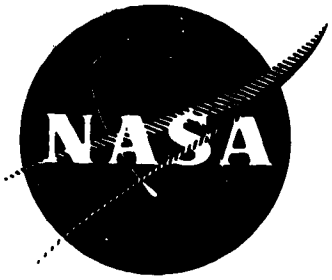

COMBUSTION OF ALUMINUM

by Seong W. Shin

prepared for

NATIONAL AERONAUTICS AND SPACE ADMINISTRATION

GRANT NGR06-002-032

REPORT NO. 4

SPACE PROPULSION PROGRAM

ENERGY CONVERSION PROGRAM

COLLEGE OF ENGINEERING

COLORADO STATE UNIVERSITY

FORT COLLINS, COLORADO

MER 66-67WRM-7

This report is a reproduction in entirety of the Master of Science thesis of Mr. Seong W. Shin. It is submitted to the sponsor and to those interested as a presentation of the technical material, and as an indication of the academic program supported by this Grant.

This research was done under NASA Research Grant NGR06-002-032 monitored by:

Dr. George Pfannebecker
Nuclear Electric Systems Division
Office of Advanced Research Technology
National Aeronautics and Space Administration
600 Independence Avenue, S.W.
Washington D.C. 20546

approved by 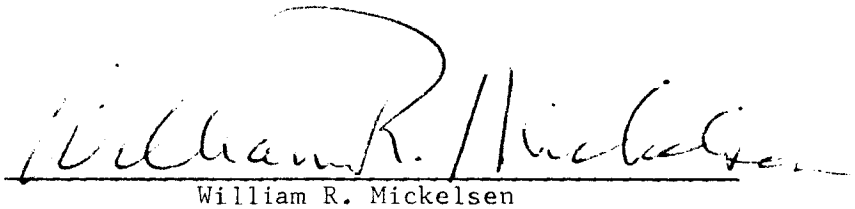

William R. Mickelsen
Professor of Mechanical Engineering
and Electrical Engineering
and principal investigator

March 15, 1967

Abstract of Thesis

Combustion of Aluminum

The purpose of this thesis is to study the following aspects of aluminum combustion and to apply the theoretical results from the study for the future designing of a colloid particle generator. The thermodynamics of the combustion of aluminum is discussed. The flame temperature and the composition of flame products at that temperature are calculated from the thermodynamic data. The radiant heat transfer from the flame is considered. The particle-size distribution is derived from the vapor-phase burning model and subsequently compared with a surface burning model. Colloid thrustor efficiencies are determined based on using particles produced from both models.

Seong W. Shin

Chemistry Department

Colorado State University

March, 1967

ACKNOWLEDGEMENTS

The author wishes to express his appreciation to Dr. G.W. Tompkin, Jr., for his guidance, patience, and consideration during the course of this work. Much of the work stems from concepts developed by Dr. Tompkin. His collaboration in formulating and carrying out this study has been invaluable. The author also wishes to thank Professor W.R. Mickelsen, Dr. J.D. Vaughan, and Dr. R.E. Carlson for their immense help, time and effort as members of the graduate committee. Financial support for this work was provided by the Electric Thrustor Systems office of the National Aeronautics and Space Administration under grant NGR 06-002-032.

THESIS

COMBUSTION OF ALUMINUM

Submitted by

Seong W. Shin

In partial fulfillment of the requirements

For the Degree of Master of Science

Colorado State University

Fort Collins, Colorado

March, 1967

CONTENTS

LIST OF TABLES

Figure

LIST OF FIGURES

LIST OF SYMBOLS

A	chamber cross sectional area, cm^2
A_t	total surface area of all particles passing position x per second, cm^2/sec
B	constant defined by Eq. (9), sec/cm
C	concentration of the oxide in the gas phase, $moles/cm^3$
C_e	equilibrium concentration of the oxide in the gas phase, $moles/cm^3$
C_i	initial concentration (before any condensation) of the oxide in the gas stream leaving the low temperature gas film adjacent to the aluminum surface, $moles/cm^3$
D^o	the dissociation energy of liquid Al_2O_3, Kcal/mole
d	chamber diameter, cm
$F(v)$	distribution function for the particle-size distribution, cm^3/sec
$f(v)$	frequency function for the particle-size distribution, $1/cm^3$
ΔG_T^o	standard Gibbs free energy change, Kcal/mole
ΔH_f^o	heat of formation from elements in an atomic gas state, Kcal/mole
K_P	chemical equilibrium constant expressed in terms of partial pressures of chemical species participating in the chemical reaction
K_1	constant defined by Eq. (49), sec

K_2	constant defined by Eq.(50), sec^2/cm^2
L	chamber length, cm
M	molecular weight of the oxide, g/mole
N	moles of gas introduced into the chamber upon burning 1 g of aluminum, assuming thermodynamic equilibrium, moles/g
n_o	number of nuclei introduced into the chamber per second per centimeter of chamber length, nuclei/sec-cm
n_t	total number of particles passing any given x plane per second, particles/second
P	chamber pressure, atm
P_{Al}	partial pressure of Al vapor
P_o	partial pressure of O vapor
P_{AlO}	partial pressure of AlO vapor
Q	constant defined by Eq.(19)
Q(T)	sensible heat between the total enthalpy of the reactants at the flame temperature, $H_{react}(T)$, and the total enthalpy of the products at the same temperature, $H_{prod}(T)$
$\dot{q}(T_B)$	net heat loss rate by radiation and conduction from the flame
R	universal gas constant, 82.057 cm^3-atm/^oK-mole
r	linear burning rate of aluminum, cm/sec
T	chamber temperature, ^oK
T_{ref}	the reference temperature, ^oK (arbitrarily set between oxide M.P. and adiobatic flame temp)

T_{ad}	adiabatic flame temperature, ^{o}K
T_P	the temperature at which the (liq → vap) phase change takes place in the flame, ^{o}K
T_B	non-adiabatic flame temperature, ^{o}K
T_{BP}^{MO}	the oxide boiling point
T_{BP}^{M}	the boiling point of metal
ΔS_T^o	the entropy change, Kcal/^{o}K-mole
u	velocity of combustion products in the chamber, cm/sec
V_n	number average particle volume, cm^3
V_v	volume average particle volume, cm^3
v	volume of a particle, cm^3
v_o	volume of a nucleus, cm^3
v_i	volume of a particle which was nucleated at x_i, cm^3
x	distance from the head end of the chamber, cm
x_i	distance from the head end of the chamber to a point of nucleation, cm
α	surface area of a particle, cm^2
α_B	the fraction of phase change accomplished
α_i	surface area of a particle at x which was nucleated at x_i, cm^2
α_o	surface area of a nucleus, cm^2
β	the degree of dissociation of liquid Al_2O_3 to the gaseous products

γ	particle growth constant defined by Eq.(3), cm/sec
δ	maximum driving force for condensation, moles/cm^3 time, sec
ρ	density of the oxide in the condensed state, g/cm^3
ρ_p	solid aluminum density, g/cm^3
Φ	accomplishment factor defined by Eq.(6)
Q'	constant defined by Eq.(61)
$\dot{m}$	the consumption rate of aluminum, g/sec.
f(m)	particle-mass distribution function, g^{-1}
η	colloid thrustor efficiency
η_u	propellant-utilization efficiency
ΣP_l	total power loss,
J	ion current density, amp./sq.m
Φ_{net}	net accelerating voltage, volt

CHAPTER I

INTRODUCTION

Current interest in combustion of aluminum stems in part from its use in colloid propulsion. The flame of aluminum vapor in an oxidizing atmosphere produces a large quantity of colloid particles consisting of submicron Al_2O_3 particles. Theoretical analyses predict that homogeneous condensation by cooling a non-reacting condensable vapor in an expansion nozzle will produce particles with less than 50% particle formation efficiency (reference 1), whereas the vapor phase combustion of certain metals (aluminum and magnesium) yields much higher percentage condensation efficiency. Condensation efficiencies in the vapor-phase combustions of Mg or Al are greatly increased by allowing the heats of combustions to radiate away from the particle-gas mixtures. Because, as the temperature reduces, the supersaturation increases. The combustion of Al or Mg gives a high flame temperature and leads to a significant radiant heat flux which is proportional to the fourth power of the absolute temperature while the nozzle-expansion systems operate at lower temperatures and lead to lower radiant heat fluxes. Recent experiment of vapor-phase combustion of magnesium by Courtney (reference 2) has shown that MgO particles are formed with 90% particle formation efficiency. However, because of the lack of satisfactory condensation theory applicable to heterogeneous condensation, the

particle formation efficiency of combustion system has not been predicted by theoretical analysis. The particle formation efficiency of aluminum combustion will be determined by experiment following this thesis. In this thesis, the following aspects of aluminum combustion are generally studied for the future construction of the Al_2O_3 colloid particle generator. Thermodynamic criterion for vapor-phase combustion of aluminum are elucidated. The flame temperature and the composition of flame products at that temperature are calculated from Thermodynamic data. Radiant heat flux is discussed. The particle-size distribution of Fein's surface burning model is compared with that of a vapor-phase burning model. For both models, the colloid thrustor efficiencies are calculated. An improved efficiency (=64%), in contrast to 30% for Fein's model, is obtained by replacing Fein's model with a vapor-phase burning model. Aluminum has been chosen as one of the reacting fuels because aluminum is available as a spent tankage in certain space missions (reference 3). The chemical reaction, $2Al(g) + \frac{3}{2}O_2(g) \rightarrow Al_2O_3(l)$, has been specifically treated in this thesis.

CHAPTER II

Thermodynamic Consideration of Aluminum Combustion

A. Distinctive Aspects of Metal Combustion

The disadvantage of using aluminum as fuel for colloid thrustor rests on its very large heat of combustion. Grosse and Conway (reference 4) stressed the relationship between position in the periodic table and heat of combustion and showed that the highest flame temperatures are to be expected with metals in groups II, III, and IV. Metal combustion produces a large amount of condensed-phase particle smoke. Most of the peculiarities of aluminum combustion arise from the production of a condensed-phase product different in composition from vapor-phase products. The large exothermic heat of formation of combustion products demands that they ultimately must become highly stable condensed-phase substances. For this reason, there exists in the combustion zone vaporized fuel and combustion products in the liquid or solid state. The dissociation of metal oxides upon vaporization generally limits the temperature of metal-oxygen flame to the boiling points of the respective metal oxides. Therefore, since the majority of metal oxides decompose partially or completely at high temperatures, the oxide boiling point used must be defined in terms of the equilibrium of the condensed oxide with its vapor-phase decomposition products at the ambient pressure. The extent of decomposition of Al_2O_3 at flame

temperatures is discussed in Section E. One of the difficulties currently encountered in the field of metal combustion lies in the lack of reliable Thermodynamic data required in the computation of decomposition equilibria. The Thermodynamic information used in this thesis has been taken from reference 5-7. In the event of conflicting data, the values of reference 5 were used.

Another distinctive characteristic of metal flames is the high emissivity, owing to the presence of condensed-phase products. Finally, it has been suggested (reference 8) that, in view of high temperatures attained in metal flames, the burnt gases should be ionized to a considerable extent. However, no measurements of ionization in metal flames have been reported, and the chemical nature of the ions is not known. A further important consequence of the presence of condensed-phase products is the possibility of sequential homogeneous and heterogeneous reaction processes in the combustion of aluminum. Heterogeneous reaction is interpreted as the reaction of aluminum suboxides or oxygen on the aluminum surface or on and within a protective aluminum oxide layer. No studies of the burning of prevaporized aluminum have been made but several excellent studies of the burning of wire and powder has been done. A thermodynamic criterion for predicting whether surface or vapor-phase burning will take place is discussed in Section B. The vapor-phase burning is commonly suppressed due to the formation of a protective oxide layer, or to

the fact that the flame temperature reduces to the temperature below the boiling point of metal by radiation, or to both causes combined.

B. Combustion of Aluminum Wire

Glassman (reference 8-9) made a survey of thermocynamic data and of the experiments on metal combustion published in the open literature. Reasoning from the thermodynamic and physical properties of metals and their oxides, he made the following generalization: (1) the flame temperature of a burning metal is generally limited to the boiling point of the oxide. (2) the existence of condensed species in the flame zone at the high temperature level makes thermal radiation important both in the rate of energy transfer from the flame to the evaporating surface and in the rate of heat loss to the surroundings. (3) In the vapor-phase diffusion burning mechanism, energy must be transferred from the flame to the metal to provide the latent heat of evaporation of the metal. Therefore, the flame zone must be at a higher temperature than the metal. If the flame temperature is the boiling point of the oxide, and the metal must be at or below the boiling point of the metal, then the required temperature difference exists only for those metals for which the boiling point of the oxide is greater than the boiling point of the metal. Applying statement (3) to the available boiling point data, Glassman predicted that Li, Na, Mg, Al, Ca, K, Be, and Si could burn in the vapor-phase. The boiling points

and melting points of the metals and those of oxides are listed in Table I. These boiling points and melting points are the temperatures measured at one atmosphere. Of course, the boiling points change with pressure; thus the question arises, since the heat of vaporization of the oxide and metal are different, will a material which will burn by one mechanism at low pressure burn by another at high pressure. This point was checked with the available thermodynamic data and Figure 1 shows that the burning character of the metals generally should not change; i.e., the lines for the metal and for the corresponding oxide do not cross as the pressure increases. A further discussion of the boiling point criterion was given by Brzustowski (reference 10).

To Glassman's condition for vapor-phase burning (the boiling point of the oxide is greater than the boiling point of metal), Brzustowski added, the second requirement for the vapor-phase burning. In any practical cases, the actual flame temperature can be reduced by radiation heat loss to a temperature below the boiling point of metal. In such cases, the metal does not vaporize and thus burns by a surface-burning mechanism. The necessary and sufficient condition added by Brzustowski is as follows: metals burn in the vapor phase when the boiling point of the oxide is greater than that of the metal and, at the same time, when the actual flame temperature is higher than the boiling point of the metal. Glassman's criterion is a

necessary but not sufficient condition for the existence of a vapor-phase flame over a burning metal. In a chemical reaction taking place at constant pressure at the temperature T, Brzustowski (reference 10) defined Q(T) as the difference between the total enthalpy of the reactants at the flame temperature, $H_{react.}(T)$, and the total enthalpy of the products at the same temperature, $H_{prod.}(T)$. Brzustowski based these quantities on a mole of that reactant which is normally called the fuel. Thus,

$$H_{prod.}(T) - H_{react.}(T) = Q(T)$$

Figure 2 shows a plot of Q(T) against T at a given pressure for three types of metals. In (a), the combustion product has no phase change between the reference temperature, $T_{ref.}$, and the adiabatic flame temperature T_{ad}. In (b), a phase change occurs at some temperature T_p lower than the adiabatic flame temperature. T_{ref} is a temperature above the oxide melting point but below the adiabatic flame temperature. T_p is the temperature at which the liquid phase oxide changes to vapor phase and is always equal to or lower than a hypothetical adiabatic flame temperature. The latent heat associated with phase change is L. In (c), the phase change occurs at the adiabatic flame temperature. $Q(T_{ref})$ is the so-called heat of combustion at the reference temperature. If α_B is defined as the fraction of phase change accomplished, the curves

of $Q(T)$ can be labelled with the appropriate values of α_B.

In (a), $\alpha_B = 0$

In (b), $\alpha_B = 0, \quad T_{ref} \leq T < T_P$

$\alpha_B = 1, \quad T_P < T \leq T_{ad}.$

$0 \leq \alpha_B \leq 1, \quad T = T_P$

In (c), $\alpha_B = 0, \quad T_{ref} \leq T < T_P = T_{ad}.$

$0 \leq \alpha_B \leq 1, \quad T = T_P = T_{ad}.$

The rate of production of sensible heat in a non-adiabatic flame at T_B is $W_f Q(T_B)$, where W_f is the molar rate of metal consumption. The net heat loss from the reaction zone can be a function of many variables such as W_f, the flame temperature, the flame emissivity, etc. However, in the case of interest, radiation and conduction from the flame are probably the most significant heat transfer mechanisms. The radiant heat transfer to an enclosure from two-phase flows has been investigated by Byrne (reference 11). However, it is very difficult to determine the numerical value of radiant heat transfer for specific case due to the very complicated nature of radiation from small particles. The peculiar nature of radiation from small particles is discussed in Chapter III in detail. In any given set of ambient conditions, the net rate of heat loss from the flame can reasonably be expressed as a function only of T_B. The net heat loss by radiation and conduction from the flame is denoted here by $\dot{q}(T_B)$. The equation which defines

the flame temperature in this non-adiabatic system is

$$W_f Q(T_B) = \dot{q}(T_B)$$

Figure 3 shows curves of $\dot{q}(T_B)$ and $W_f Q(T_B)$ versus T_B for the three cases shown previously. The intersection of the two curves gives the non-adiabatic flame temperature. Here, T_B is the non-adiabatic flame temperature at which the rate of heat production is equal to the rate of heat loss. In case (a), α_B is known to be zero and the flame temperature is T_{B_1}. Clearly, $\alpha_B = 0$ for all $T_{ref} \leqslant T_{B_1} \leqslant T_{ad}$. In case (b), three examples are possible:

$$\alpha_B = 0 , \qquad T_{ref} \leqslant T_{B_1} < T_P$$

$$0 \leqslant \alpha_B \leqslant 1 , \qquad T_{B_2} = T_P$$

$$\alpha_B = 1 , \qquad T_P < T_{B_3} \leqslant T_{ad}$$

The three examples occur in order of decreasing $\dot{q}$. In case (c), only two types of solutions are possible:

$$\alpha_B = 0 , \qquad T_{ref} \leqslant T_{B_1} < T_P$$

$$0 \leqslant \alpha_B < 1 \qquad T_{B_2} = T_P = T_{ad}$$

Only positive values of $\dot{q}$ have been considered, because, if $\dot{q}$ is negative, heat is transferred to the flame from its surroundings. The above examples are now applied to the combustion of metals. If T_{ref} is taken as the temperature above the oxide melting point, then $T_P = T_{BP}^{MO}$ is the

oxide boiling point, and α_B is the fraction of oxide vaporized. Case (a) shows a metal whose temperature of flame is always less than T_{BP}^{MO} and whose product of combustion is liquid oxide. In (b), the flame temperature can exceed T_{BP}^{MO} under adiabatic conditions with the oxide completely vaporized. Case (c) shows a metal whose adiabatic flame temperature can not exceed T_{BP}^{MO}. The product oxide is only partially vaporized under adiabatic conditions. The criterion for vapor-phase combustion is that T_B exceeds T_{BP}^{M}. Here T_B is the flame temperature and T_{BP}^{M} is the boiling point of metal. Metals (a), (b) and (c) can therefore all burn in the vapor-phase if $T_B > T_{BP}^{M}$. Since T_B depends upon the net heat loss to the surroundings, the existence of vapor-phase mechanism is also a function of the heat transfer between the particle and its environment. Calculations of adiabatic flame temperatures reported by Glassman (reference 9) and Fassell (reference 12) show that Al, Be, Li, and Mg fall into category (c). The adiabatic flame temperature is reported (reference 4) to be equal to the boiling point of various oxides involved. Fassell made the computer calculations of the adiabatic flame temperature and the mole fraction of the species present at this temperature. His results are presented in Table II. Fassell pointed out that, if radiation losses occur from the burning droplet of metal, the temperature will be reduced with a corresponding increase in the liquid oxide species because the degree of supersaturation of

vapor becomes greater with reduced temperature. Fassell also identified the combustion product of aluminum by the X-ray diffraction method (major oxide species is Alpha-Al_2O_3 and minor species is Gamma-Al_2O_3). Rautenberg and Johnson (reference 13) have measured the flame temperature in the aluminum oxygen reaction and have verified that it is equal to the boiling point of Al_2O_3 (within a few hundred degrees of 3800°K). They also indicated that the emitting source in an aluminum photoflash lamp is actually a blackbody at 3800°K and that this temperature can not be altered substantially. The criterion for vapor-phase combustion has been verified by Brzustowski in his experimental work with aluminum. Aluminum also satisfies Glassman's criterion. Literature review shows that, as long as aluminum burns at low pressure and high oxygen concentration, fine aluminum wires or small aluminum particles burn in the vapor-phase. The heat requirement for the Al vaporization would be eliminated, if aluminum wires burn in vapor-phase , for the wires would self-vaporize due to the heat transfer from the flame zone. In this sense, a wire burning technique seems particularly attractive in the combustion of aluminum. In summary, aluminum burns in a vapor-phase according to the criterion of both Glassman and Brzustowski. It has been verified by Brzustowski that metals can be divided into three categories, depending on the relationship of the adiabatic flame temperature to the boiling point of oxide. The

effect of heat loss from the flame on its temperature has been discussed in detail, and it was concluded that the oxide boiling point may be upper limit on the actual flame temperature even if the adiabatic flame temperature could be higher. In contradiction to Glassman's conclusion that the burning character of metals generally does not change upon the pressure, Brzustowski pointed out that the same metal may conceivably burn in the vapor phase in one environment and on the surface in another, depending upon the net rate of heat loss from the flame zone. This point was verified by Brzustowski's experiment with aluminum wire. A map of the burning mechanisms observed by Brzustowski in oxygen-argon mixtures is shown in Figure 4. The observations were made at various pressures ranging from 100 mm Hg to 225 psia and at values of the oxygen mole fraction varying in steps of 0.1 between 0 and 1. Additional low pressure tests were carried out at 50 mmHg for various oxygen mole fractions. A wire burned in vapor-phase flames only in region 3 in Figure 4. Therefore, the theoretical vapor-phase model can not apply in the rest of regions. It may be concluded that aluminum wire burns in the low pressure (below 500 mm Hg) as can be seen in Figure 4. Vapor-phase combustion of aluminum wire was also verified by Harrison and Yoffee (reference 17). In their experiments, aluminum wires were found to burn with a diffuse combustion zone and produce large quantities of oxide smoke, indicating a vapor-phase burning process. Kirschfeld's

investigations of burning aluminum wire (reference 18) indicated a vapor-phase burning process. In his experiment, an increase of burning rate with decreasing chamber pressure below 0.5 atmosphere was observed.

C. Combustion of Aluminum Particles in a Hot Oxidizing Atmosphere

Brzustowski and Glassman (reference 30) correlated the observed behavior of non-volatile metal (Al, Be, Si, Ti, Zr, B) particles burning in a hot oxidizing gas with the physical properties of metals and their oxides. Table I shows the melting and boiling points of the metals and of their oxides. Most of the data in Table I are taken from the JANAF thermochemical data (reference 6). The oxides of all the volatile metals listed in Table I are porous and not able to seal the metal against surface oxidation. This property is shown in the last column which lists the ratio of the volume of oxide formed to the volume of metal consumed. It is more than a density ratio because it takes into account the weight of oxygen consumed. When this number, often referred to as the Piling and Bedworth ratio, is less than unity, the oxide is porous. When it is much larger than unity, of the order of 3, there is a tendency for the oxide to blister and peel away from the surface. A value close to unity, of the order of 1.3, indicates a good protective layer. Brzustowski and Glassman observed from Table I that: (1) the metals are

classed according to the properties of the oxides which characterize the burning mechanism. The oxides of Al, Be, Si are protective materials that adhere well to the metal surface. It is expected that an oxide layer on the surface of these metals largely inhibits oxidation over a wide temperature range. The volume ratios of the oxides of Al, Be, Ti, and Zr are all larger than unity but not so large that the oxide coating might be expected to blister and peel off the metal surface. (2) the oxides of Al, Be, Ti and Zr boil at temperatures exceeding the boiling points of the respective metals. The criterion for vapor-phase burning indicates that Al, Be, Ti and Zr can burn in the vapor-phase diffusion flames by which means that gas-phase oxidants or aluminum suboxides diffuse into the aluminum oxide layer. Figure 5 shows the scheme postulated to explain the observed burning behavior of Al, Be, and Si. The rate of heat transfer from the surrounding gas to a large particle is low enough so that a layer of oxide has time to build up on the surface before the particle melts. In other words, the time required to heat and melt the larger particles is longer than the smaller particles. This layer greatly inhibits further oxidation, so that ignition does not take place. Indications are that in the combustion gases given off from the surface of a burning solid aluminum particles larger than about 80 microns behave in this way (reference 15). If the metal particle is small enough, the rate of heat transfer to the

particle is generally high, and melting occurs before appreciable surface oxidation has taken place. The net rate of heat loss from the surface of the oxide layer determines the burning mechanism. Furthermore, if the surrounding atmosphere is hot enough and the residence time of the particles in it is long enough, it is possible that the metal within the liquid oxide shell may reach its boiling point. It then becomes slightly superheated and bursts the shell. The hot metal droplets released in this fragmentation can burn by the vapor-phase diffusion mechanism. From Gordon's observations (reference 16), it may be estimated that aluminum particles of about 50 microns exhibit this behavior in a 2800°K oxidizing gas.

D. Ignition Temperature of Aluminum Powder

The ignition of a metal in a reactive atmosphere is a phenomenon involving heat transfer and chemical reaction at the surface. Reynolds (reference 14) performed an analysis that relates the ignition temperature with the low temperature oxidation properties of the metal. The treatment is based on the generally accepted view that ignition will occur if the heat produced by the oxidation reaction exceeds the heat losses to such an extent that the temperature rise continues at an accelerating rate. Reynolds considers both conductive and radiative heat losses. As he uses only one dimensional expressions, the analysis applies only to the ignition of metal in bulk.

Grosse and Conway (reference 4) reported ignition temperatures of various metals, measured partly by others and partly in their own works. Ignition temperatures of metals in oxygen are shown in Table III. Grosse and Conway also state that among the factors that may affect the ignition temperature are the following: purity of the metal, gas composition including moisture content, pressure, state of subdivision, previous history of the metal, and apparatus and technique. The ignition temperature can be defined as the surface temperature of either the particle or the bulk at which the rate of heat gain from a chemical reaction first becomes equal to the net rate of heat loss from the surface. The rate of heat loss from the surface is the sum of conductive, convective, and radiant rates. The rate of heat loss from the surface by conduction into the interior depends on the conductivity, size, and past history of the particles. The rate of convective heat loss from the surface depends only on the surface temperature and ambient fluid. The rate of radiant heat loss depends on the surface temperature of the particle, the extent of chemical reaction reached, the emissivity of particles, and the concentration of thermal radiators in the surroundings. A plot of the net rate of heat loss and the rate of heat gain from chemical reaction against surface temperature in Figure 6 as was shown in reference 10 serves to define the concept of ignition temperature. The ignition temperature is the temperature at which the

heat balance between the rate of heat gain and the rate of heat loss is achieved. Once the ignition temperature has been exceeded, the temperature jumps to a stable temperature such as the flame temperatures, T_{B_1}, T_{B_2}, and T_{B_3}, in Figure 3. The heat release rate shown by curve $\dot{q}_{react.1}$ corresponds to a reaction which is limited only by the surface temperature. Surface reactions which form porous, non-protective oxides fall into this category. Curve $\dot{q}_{react.2}$ shows the rate of heat gain from a reaction which is completely inhibited below some critical temperature. If the temperature-limited reaction rate at that critical temperature exceeds the rate of heat loss, ignition occurs. T_{ig2} corresponds, for instance, to the melting point of the protective aluminum oxide film. Ignition of first particles may occur very slowly. The ignition of subsequent particles is accelerated by the heat release from those particles which are burning. The ignition of single aluminum particles injected into a hot gas stream of known uniform temperature, composition, and flow velocity were investigated by Friedman and Macek (reference 19). It was found that injected particles would only ignite under certain conditions. Their experimental results for ignition temperature under the various ambient conditions are shown in Figure 7. From the figure, it can be easily seen that ambient oxygen content is a relatively unimportant variable within the range of 5-25% O_2 mole fraction, but an ambient gas temperature of about 2300°K is the necessary condition

for ignition. This almost coincides with the melting point of aluminum oxide (2318°K). Friedman and Macek concluded that ignition occurs only upon melting of the oxide layer which coats aluminum. It is assumed that melting of protective oxide layer causes a discontinuous increase in the surface reaction rate, leading to ignition.

E. The Flame Temperature and Chemical Species Existing at the Temperature

Wolfhard and Parker (reference 20) compared flame temperatures measured by line-reversal and absolute-intensity methods with color temperatures. The former methods gave temperatures of about 3273°K, whereas the color temperature was 3873°K for aluminum. The discrepancy was explained by anomalous absorptivity of the small aluminum oxide particles which was found to increase from small values in the visible to unity at about 3000 Angstrom. Based on value of the aluminum oxide boiling point (3253°K) available at the time of their work, the authors concluded that the true flame temperature was that determined by the line-reversal and the absolute-intensity methods, whereas the color temperature had no physical significance. In comparison with the now accepted value of aluminum oxide boiling point of 3800°K (reference 21), the boiling point of aluminum oxide is closer to the measured color temperature (3873°K). A plausible explanation might be that the temperature of the aluminum flame was reduced below the theoretical maximum by radiation losses. In contrast to Wolfhard and

Parker, Rautenberg and Johnson (reference 13) identify the color temperature with the true flame temperature. In any case, the flame temperature can not exceed the oxide boiling point because of the restriction that large heat of vaporization of oxide, which includes a heat of decomposition of Al_2O_3 to lower oxides. A higher environmental pressure would therefore give a slightly higher flame temperature because of a slightly higher boiling point at that higher pressure. This occurrence of dissociation at high temperature complicates the calculation of theoretical flame temperature. This theoretical temperature to which the flame may rise after the combustion can be calculated from the thermodynamic data. It is necessary to have a flame temperature to be able to calculate the amount of dissociation and obtain the gas composition. On the other hand, the temperature itself depends on the composition. The theoretical flame temperature is only obtained on the assumption that there is no heat loss or gain by radiation, thermal conduction, or convection. The first step is to calculate the composition of the flame products for an assumed temperature. The next step is to find the amounts of heat produced by the chemical reaction and heat consumed to heat the flame products of the composition to the assumed temperature. The assumption of flame temperature is repeated until the heat balance between heat production and heat consumption is achieved. The identification of chemical species existing at the flame temperature

is still in doubt. Friedman and Maček in their experimental work on aluminum particle combustion showed the presence of decomposition products, Al, AlO, Al_2O, O, and O_2 at one atmosphere. Glassman, however, argues that Al_2O species does not exist. In Glassman's spectroscopic investigation of burning aluminum wires in oxygen-inert gas mixtures, all bands and lines on the aluminum flame spectrograms are identifiable as Al, AlO, and impurities, and none can be attributed to Al_2O. The only possibility that could resolve this disagreement would be for Al_2O to be present as a short-lived intermediate under the condition that aluminum flame experiments are carried out. From a vapor pressure study of the aluminum-oxygen system under reducing and under neutral conditions, Brewer and Searcy (reference 21) concluded that under reducing conditions Al and Al_2O are the principal vapor species, while under neutral conditions AlO and O are the principal vapor components. In the reducing conditions, Al_2O_3 is heated with aluminum or another reducing metal. To achieve neutral conditions, Al_2O_3 is heated alone. Following Glassman and Brewer and Searcy's observations, it can be assumed that one mole of $Al_2O_3(l)$ dissociates into four moles of the fragments AlO, Al, and 2[O] upon decomposition. The assumption that atomic rather than molecular oxygen is the remaining fragment was made following Ackermann, Thorn, and Winslow (reference 22). The formation and the decomposition reactions of $Al_2O_3(l)$ are:

Formation of $Al_2O_3(l)$

$$2Al(g) + \frac{3}{2} O_2(g) \longrightarrow Al_2O_3(l)$$

Decomposition of $Al_2O_3(l)$

$$Al_2O_3(l) \longrightarrow AlO(g) + Al(g) + 2O(g)$$

At the equilibrium between liquid phase and gaseous phase of burnt products, the number of moles of undecomposed $Al_2O_3(l)$ is $n(1-\beta)$, whereas the numbers of moles of $AlO(g)$, $Al(g)$, and $O(g)$ are $n\beta$, $n\beta$, and $2n\beta$, respectively. β is defined as the degree of dissociation and n is the total number of moles of $Al_2O_3(l)$ initially produced by combustion. The sum of moles of each species at equilibrium gives the total number of moles, that is $n(1+3\beta)$ moles. The adiabatic flame temperature is now determined by successive approximations. First, trial calculation is attempted using the flame temperature of 3800°K. The equilibrium constant K_P is expressed for the decomposition reaction of $Al_2O_3(l)$ in terms of the partial pressures of each species.

$$K_P = P_{AlO}\, P_{Al}\, (P_o)^2$$
$$= 4(P_{Al})^4$$

The value $P_{Al} = 8.9 \times 10^{-2}$ atm can be obtained using $\text{Log}_{10}K_P = -3.6$ at T = 3800°K (Figure 8). The partial pressure is proportional to mole fraction and therefore, $P_{Al} = \frac{n\beta}{n(1+3\beta)} \cdot P$ where P is the total pressure. The degree of dissociation at T = 3800°K thus found from the above relation is $\beta = 0.12$. The numbers of moles of burnt

products on the basis of one mole $Al_2O_3(l)$ formation are as follow:

Burnt product	number of mole
$Al_2O_3(l)$	0.88
$Al(g)$	0.12
$AlO(g)$	0.12
$O(g)$	0.24
Total	1.36

It is noted here that the true mole number of burnt products is $n(1 + 3\beta) = 1.36n$, an increase of $0.36n$ moles over the mole number of burnt products without decomposition. This directly indicates that the dissociation uses up a significant amount of energy and limits the flame temperature. The dissociation energy of $Al_2O_3(l)$ is indirectly determined by the use of thermochemical data in reference 5.

$$\begin{array}{lll} Al(g) + O(g) \longrightarrow AlO(g) & & \Delta H^o_{f_1} \\ -2Al(g) + 3O(g) \longrightarrow Al_2O_3(l) & & \Delta H^o_{f_2} \\ \hline Al_2O_3(l) \longrightarrow AlO(g) + Al(g) + 2O(g) & & \Delta D^o \end{array}$$

Thus, the dissociation energy per mole of $Al_2O_3(l)$ is

$$\Delta D^o = \Delta H^o_{f_1} - \Delta H^o_{f_2} = 562.59 \text{ Kcal/mole}$$

where ΔH^o_f is the heat of formation from elements in an atomic gas state. The energy consumed upon the decomposition of 0.12 moles (β) of $Al_2O_3(l)$ is therefore 67.51 Kcal

($=\beta \Delta D^{o}$). We next calculate how much heat would be required to heat the combustion products from room temperature to T=3800°K. The heat content of the total true moles of combustion products thus calculated is 135.25 Kcal. We next calculate how much heat is produced in the flame. The main source of heat liberated is in the formation of $Al_2O_3(l)$ and is equal to one molar heat of formation of $Al_2O_3(l)$ at room temperature from the assigned reference elements (ΔH_f^o = -400.4 Kcal/mole at 298°K, reference 5). The value of ΔH_f^o = -400.4 Kcal/mole compares with 135.25 Kcal of heat consumption; thus, the true temperature of the flame, assuming no heat loss, will be higher than 3800°K, and we must repeat the whole calculation for composition for a higher temperature and then repeat the heat balance test and so on until a temperature is found for which the heat consumed is equal to the heat produced in forming a burning mixture with the composition at that temperature. The computations of compositions of aluminum-oxygen flame at various temperatures and the heat balance computations are summarized in Table IV. From the table, it can be concluded that the theoretical adiabatic flame temperature lies near 3980°K. This discrepancy between the reported flame temperature, 3800°K, and the temperature in this calculation, 3980°K, probably results from the extrapolation to high temperatures of thermodynamic data in reference 5. This flame temperature is comparable with the flame temperature of 3908°K in Table II calculated by Fassell (reference

12). However, the actual flame is expected to be much lower than the adiabatic flame temperature because of large amount of radiant heat loss from the flame due to the great emissivity of the particles in the flame. The thermodynamic data in reference 5 relevant to the calculations in this section are listed in Table V. The plots of the Gibbs free energy change (ΔG_T^o), the enthalpy change (ΔH_T^o), and the entropy change (ΔS_T^o) against the absolute temperature in Kelvin are shown in Figures 9, 10, and 11 for the decomposition reaction, $Al_2O_3(l) \longrightarrow AlO(g) + Al(g) + 2O(g)$ based upon the data in Table V. From these figures, the $Log_{10}K_P$ versus T^oK graph is plotted in Figure 8 by the thermodynamic relationship, $Log_{10}K_P = -\frac{\Delta G_T^o}{2.303RT}$.

CHAPTER III

Radiant Heat Transfer in Aluminum-Oxygen Flame

The flame of aluminum-oxygen contains a large quantity of small Al_2O_3 particles. Hot gases are selective in their emission, leaving blanks in their spectra, whereas particles are continuous emitters, and for this reason the liquid or solid particles emit much more energy for a given temperature. In the analysis of radiant heat transfer from Al-O flame, Byrne (reference 11) neglects the radiant heat loss from gaseous aluminum flame products on the ground of selectivity in their emission. In order to investigate the mechanisms of excitation of the continuum and the AlO spectra in the aluminum-oxygen combustion reaction, Rautenberg and Johnson (reference 13) vaporized aluminum foil in oxygen by means of an electric current pulse and examined the emitted radiation by time-resolved spectroscopy. They concluded that the principal light emission is blackbody radiation from AlO and Al_2O_3 at or below 3800°K, that is, the emissivity is unity. However, this conclusion that the radiation of aluminum flame is identical with that of a black-body can not be accepted without reservation. There are two reasons for this. First, the emissivity of the material of the particle may vary with wavelength and is a complicated function of particle size, the particle concentration, and the surrounding pressure. The second reason is associated with the scattering of

light by small particles; the particles which are smaller than a wavelength of light will not only scatter, but will absorb with an absorption coefficient which also depends on wavelength even if the material of the particle is black or grey. There has been little information in the open literatures on the numerical evaluation of radiation energy from the flame. Recently, Byrne (reference 11) has investigated radiant heat transfer from hot solid or liquid combustion products to the walls of a combustion chamber in an analytical method. Radiation heat transfer from the combustion of aluminum in an oxygen containing atmosphere under the high pressure was investigated. It should be noted here that the results of his investigation can only be regarded as a representative trend concerning the relative importance of several parameters. The assumptions he made are: (1) the particles are randomly distributed throughout a transparent gas in the combustion chamber; (2) the particle cloud is isothermal; variations of particle temperature with radial distance because of energy absorption by the wall and the variation of incident radiation caused by position in the particle cloud are negligible; (3) all the particles are black, spherical, of equal size and at the same temperature; (4) the wall of combustion chamber is isothermal and is diffuse in both emission and reflection. The primary point of interest was a prediction of the radiant heat transfer. Parametric variations were made to determine the effects of particle size, chamber

pressure, wall reflectivity, wall temperature, and particle mass fraction. The number of particles of Al_2O_3 per unit volume is specified indirectly by choosing a particle mass fraction of the mixture. The fraction of condensed Al_2O_3 particle mass to the mixture is defined as the particle mass fraction. Figure 12 is a plot of heat flux versus particle size. The effect demonstrated here is that, all else being equal, the larger the particle size, the smaller the radiant heat transfer to the wall. As the particle size is increased, the total radiating surface area is decreased because of a decrease in the area to volume ratio as size is increased. Since the total amount of energy radiated is directly proportional to the surface area, a change in surface area brings about a similar change in the total energy emitted. It is interesting to note from the changing slope of the curve, that as the particle size is increased, the wall heat flux becomes increasingly insensitive to further increase in particle size. Figure 13 is a plot of heat flux versus pressure. The indicated trend is that higher pressures cause greater radiant heat flux to the wall. As the chamber pressure is increased, the flame becomes more dense, more Al_2O_3 particles are in the chamber, and therefore more total energy is emitted. Figure 14 indicates that heat flux is strongly affected by wall reflectivity. Reflectivity is a fraction of incident flux which is reflected. As the energy is reflected by the wall, it is forced to traverse the absorbing fluid many

times before the energy is absorbed by the wall. The longer effective path length, therefore, causes more of the initial flux to be absorbed by the cloud as the reflectivity of the wall is increased. The dashed portion of the curve indicates known boundary conditions; as the wall reflectivity reaches unity, no heat flux is absorbed by the wall. It may be seen in Figure 15 that the wall heat flux is almost independent of the wall temperature. The driving potential in radiant heat transfer is the fourth power of temperature. In this case, the particle temperature is so high that the fourth power of this temperature is very large compared with the fourth power of the wall temperature, regardless of wall temperature. Figure 16 shows the effect of the particle mass fraction on the apparent emissivity. Apparent emissivity is taken as the initial incident flux density to the wall from the particles divided by the initial heat flux density from a black-body at the particle temperature. Theoretically, as the particle mass fraction becomes very large, the apparent emissivity of the particle cloud should approach unity in the limiting case, because, as the particle mass fraction approaches unity, the system becomes a black solid cylinder enclosed by the chamber wall. In other words, an element of the wall can no longer see anything but particles. In Figure 16, the curve falls off to an apparent emissivity of zero when the particle mass fraction is unity. Byrne's results are obviously in error above a particle mass

fraction of about 15%. Byrne's assumption (2) is over-simplified. In fact, the temperature along the chamber changes with radial distance due to the large quantity of radiant heat loss from the flame. From the view point that assumption (2) can not be justified in actual system, Byrne's numerical results can not be accepted in the practical case of aluminum combustion. However, his data are very useful in predicting the general trend of the radiant heat transfer with the variation of parameters. The numerical analysis of radiant heat transfer from aluminum flame seems extremely difficult at the present time because of the unknown scattering and absorbing behavior of small Al_2O_3 particles in the flame. Figures 12, 13, 14, 15 and 16 are the results of Byrne's analysis. The Byrne's analysis does however provide some guidance for the analysis of the model of this research.

CHAPTER IV

Aluminum Oxide Particle Size Distributions

The information about the particle size distribution of Al_2O_3 is required to predict the ideal colloid thrustor efficiency. A theoretical model has been derived by Fein (reference 24) to analyze the oxide particle size distributions obtained by burning cyclindrically perforated aluminum with oxygen.

A. Description of the Model and Assumptions by Fein

The Fein's physical model is schematically pictured in Figure 17. The assumptions made by Fein in his analysis are; (1) complete radial mixing is assumed throughout the chamber except within a thin low temperature region immediately adjacent to the aluminum surface; (2) steady state is assumed to prevail, and the pressure and temperature are assumed constant throughout the main gas stream; (3) because of the increase in burning surface area with increasing the distance from the head end of the chamber (x), it is assumed that the velocity of the combustion products is directly proportional to x. This velocity is given by Eq. (1);

$$u = N\rho_{pr}\left[\left(\frac{\pi_d}{A}\right)\left(\frac{RT}{P}\right)\right] x \qquad (1)$$

where

u = velocity of combustion products, cm/sec

N = moles of gas introduced into the chamber upon burning

1 gram of aluminum, g-moles/g aluminum

ρ_p = solid aluminum density, g/cm^3

r = linear burning rate of aluminum, cm/sec

d = chamber diameter, cm

A = chamber cross sectional area, cm^2

R = universal gas constant, 82.057(cm^3)(atm)/($^\circ$K)(g-mole)

T = chamber temperature, $^\circ$K

P = chamber pressure, atm

(4) it is assumed that the particles are nucleated at a constant rate of n_o (nuclei/sec/cm of the chamber length). The total number of particles passing any given distance x, n_t, is given by Eq. (2).

$$n_t = n_o x \tag{2}$$

(5) particles are assumed to grow by the mechanism of diffusion of gaseous aluminum, atomic oxygen, and aluminum suboxides to the particle surface followed by a heterogeneous chemical reaction to form condensed Al_2O_3. The rate of particle growth is given by the mass transfer law, Eq.(3).

$$\frac{dv}{d\theta} = \gamma (c-c_e)\alpha \frac{m}{\rho} \tag{3}$$

where

γ = an empirical rate constant which will be referred to as the growth constant, cm/sec

c = concentration of the oxide in the gas phase, moles/cm^3

C_e = equilibrium concentration of the oxide in the gas phase at the chamber pressure and temperature, moles/cm^3

α = surface area of a particle assuming that the particle is spherical, cm^2

v = volume of a single particle, cm^3

M = molecular weight of the oxide, g/g-mole

ρ = density of the oxide in the condensed state, g/cm^3

θ = time, sec

Fein assumes that the growth constant, γ, is constant and independent of particle radius. Fein justifies the above five assumptions by demonstrating the agreement between the model and experimental data.

B. Derivation of Average Particle Volumes and the Particle Size Distributions

Fein derived the particle size distribution from his model shown in Figure 17. First, he took the differential mass balance of the gaseous oxide taken over the gas stream. The small differential element of chamber length is shown in Figure 18. The flow rate of oxides into this differential element is CAU moles/sec. The flow rate of oxides from this element to the main stream is CAU + $\frac{d}{dx}$(CAU)dx moles/sec. Fein defines C_i (moles per cubic centimeter) as the initial concentration (before any condensation) of the oxides leaving the gas film adjacent to the aluminum surface. The flow of condensable gaseous oxides into this differential element

from the aluminum surface is given by:

$$C_i Au = C_i A \left[N \rho_p r \left(\frac{\pi d}{A}\right)\left(\frac{RT}{P}\right) \right] dx$$

$$= C_i N \pi d \rho_p r \left(\frac{RT}{P}\right) dx \text{ moles/sec}$$

A_t is defined as total surface area of all particles at the position of x per second. Then the total particle surface area per cubic centimeter at position of x is A_t/Au cm^2/cm^3, and the total surface area of all particles in the differential element is $(A_t/Au)(Adx) = A_t dx) = A_t dx/u$. From Eq. (3), the total number of moles of oxides that condense in the differential element per second can be expressed by the following equation:

$$\frac{\rho}{M} dv = \gamma (C-C_e) \alpha d\theta$$

$$= \gamma (C-C_e) \frac{A_t dx}{u}$$

The amount of oxide condensate is equal to the sum of the flows into the differential element from gas stream and from the gas film adjacent to the aluminum surface minus the flow out from the differential element to the main gas stream,

$$CAU + C_i N \pi d \rho_p r \left(\frac{RT}{P}\right) dx - \left[CAU + \frac{d}{dx}(CAU) dx \right]$$

$$= \gamma (C-C_e) A_t \left(\frac{dx}{u}\right) \qquad (4)$$

Substituting u of Eq. (1) into Eq.(4) gives:

$$\frac{C_i N\pi d\rho_p rRT}{P} - \frac{N\pi d\rho_p rRTx}{P}\frac{dc}{dx} - \frac{CN\pi d\rho_p rRT}{P} = \frac{\gamma(C-C_e)A_t AP}{N\pi d\rho_p rRTx} \quad (5)$$

The accomplishment factor Φ is defined as:

$$\Phi = \frac{C_i - C}{C_i - C_e} \quad (6)$$

The maximum driving force δ is defined as:

$$\delta = C_i - C_e \quad (7)$$

Substituting $C = C_i - \delta\Phi$ and $\frac{dc}{dx} = -\delta\frac{d\Phi}{dx}$ into Eq. (5) and using $A = \pi(\frac{d}{2})^2$ yields:

$$\frac{d}{dx}(x\Phi) + \frac{BA_t(\Phi - 1)}{x} = 0 \quad (8)$$

where

$$B = (\frac{\gamma}{4\pi})(\frac{P}{N\rho_p rRT})^2 \quad (9)$$

Eq. (8) is the differential equation expressing the mass balance for the oxide around a differential element of the chamber. Next step is to express A_t as a function of x and Φ, and then find a solution to Eq.(8). Let v_i be the volume of a particle (cubic centimeter) at the position of x, and let a_i be the surface area (centimeter squared) of this particle. v_o and a_o are the values of v_i and a_i, respectively, at the position of $x = x_i$. Here x_i is the distance from the head end of the chamber to a point of nucleation. If the particles are spherical, then:

$$v_i = \left(\frac{\pi}{6}\right)\left(\frac{\alpha_i}{\pi}\right)^{\frac{3}{2}} \tag{10}$$

and

$$dv_i = \frac{1}{4}\left(\frac{\alpha_i}{\pi}\right)^{\frac{1}{2}} d\alpha_i \tag{11}$$

Furthermore, from the growth law given by Eq. (3),

$$dv_i = \left[\gamma (C-C_e)\alpha_i \frac{M}{\rho}\right] d\theta \tag{12}$$

From Eq.(1),

$$u = \frac{dx}{d\theta} = N\rho_p r \left[\left(\frac{\pi d}{A}\right)\left(\frac{RT}{P}\right)\right] x$$

$$d\theta = \frac{AP}{N\pi\rho_p r dRT} \quad \frac{dx}{x} \tag{13}$$

By the substitution of Eq.(13) into (12), the independent variable changes from time to distance as follows:

$$dv_i = \left[\frac{\gamma (C-C_e)\alpha_i MAP}{\rho N\rho_p r \pi dRTx}\right] dx \tag{14}$$

If dv_i is eliminated between equations (11) and (14),

$$\frac{1}{4\sqrt{\pi}}\alpha_i^{-\frac{1}{2}} d\alpha_i = \left[\frac{\gamma (C-C_e)MAP}{\rho N\rho_p r \pi dRTx}\right] dx \tag{15}$$

Eq. (15) is integrated between the limits (α_o, x_i) and (α_i, x),

$$\alpha_i^{\frac{1}{2}} = \int_{x_i}^{x} \left[\frac{2\sqrt{\pi}\,\gamma\,(C-C_e)MAP}{\rho N\rho_p r RT \pi d}\right]\frac{dx}{x} + \alpha_o^{\frac{1}{2}} \tag{16}$$

Substituting $A = \pi\left(\frac{d}{2}\right)^2$ into Eq.(16) and squaring,

$$\alpha_i = \left[\int_{x_i}^{x} \frac{\sqrt{\pi}\,\gamma (C-C_e) MPd}{2\rho N \rho_p r R T} \frac{dx}{x} + \alpha_o^{\frac{1}{2}} \right]^2 \qquad (17)$$

The expression for α_i is obtained after substituting the relation, $C-C_e = \delta\,(1-\Phi)$, into Eq.(17);

$$\alpha_i = \left[Q \int_{x_i}^{x} (1-\Phi)\,\frac{dx}{x} + \alpha_o^{\frac{1}{2}} \right]^2 \qquad (18)$$

where

$$Q = \frac{\sqrt{\pi}\,\gamma \delta\, MPd}{2\rho N \rho_p r R T} \qquad (19)$$

Eq.(2) indicates that the number of particles passing any given position of x is $n_o x$. Accordingly, the number of particles initiated per second over the x interval dx_i is $n_o dx_i$. The surface area of particles passing position of x per second initiated over the x interval dx_i is $n_o \alpha_i dx_i$. The total surface area of all particles passing position of x per second (A_t) is the integration of $n_o \alpha_i dx_i$ from o to x,

$$A_t = n_o \int_{o}^{x} \alpha_i dx_i \qquad (20)$$

If the α_i of Eq.(18) is substituted into Eq.(20), the resultant equation is the function for A_t expressed in terms of Φ and x. If Eq.(8) is expanded and solved for $\frac{d\Phi}{dx}$,

$$\frac{d\Phi}{dx} = \frac{BA_t(1-\Phi)}{x^2} - \frac{\Phi}{x} \qquad (21)$$

If Eq.(21) is solved for A_t, assuming Φ is constant ($\frac{d\Phi}{dx} = 0$),
the result is:

$$A_t = \left[\frac{\Phi}{B(1-\Phi)}\right]x \qquad (22)$$

Upon integration of Eq.(18) assuming Φ is constant, we obtain:

$$\alpha_i = \left[Q \int_{x_i}^{x} \frac{1-\Phi}{x} dx + \alpha_o^{\frac{1}{2}} \right]^2$$

$$= \left[Q(1-\Phi) \ln\left(\frac{x}{x_i}\right) + \alpha_o^{\frac{1}{2}} \right]^2$$

$$= Q^2(1-\Phi)^2 \left[\ln\left(\frac{x}{x_i}\right)\right]^2 + 2\alpha_o^{\frac{1}{2}} Q(1-\Phi) \ln \left(\frac{x}{x_i}\right) + \alpha_o \qquad (23)$$

If Eq.(20) is integrated after substituting Eq.(23) into Eq.(20),

$$A_t = \int_o^x n_o \alpha_i dx_i$$

$$= \left[2n_o Q^2(1-\Phi)^2 + 2n_o \alpha_o^{\frac{1}{2}} Q(1-\Phi) + n_o \alpha_o\right] \qquad (24)$$

Elimination of A_t from Eqs.(22) and (24) yields:

$$\frac{\Phi}{Bn_o} = 2Q^2(1-\Phi)^3 + 2\alpha_o^{\frac{1}{2}} Q(1-\Phi)^2 + \alpha_o(1-\Phi) \qquad (25)$$

Now, the number and volume average particle sizes and frequency function for the particle-size distribution will be

derived. The number average particle volume, V_n, is defined as the total particle volume in a sample divided by the number of particles in that sample. If L is the chamber length, the total particle volume leaving the chamber is:

$$\int_o^L n_o v_i(x_i,L)dx_i \tag{26}$$

where $v_i(x_i,L)$ is the volume of a particle at x=L nucleated at $x=x_i$. The total number of particles leaving the chamber per second is n_oL, and therefore the number average particle volume V_n is given by:

$$V_n = \frac{1}{n_oL}\int_o^L n_o v_i(x_i,L)dx_i \tag{27}$$

From the Eqs.(10) and (18), $v_i(x_i,L)$ can be found:

$$v_i(x_i,L) = \left[\frac{1}{6\sqrt{\pi}}\right]\left[Q\int_{x_i}^{L}(1-\Phi)\frac{dx}{x} + \alpha_o^{\frac{1}{2}}\right]^3$$

$$=\left[\frac{1}{6\sqrt{\pi}}\right]\left[Q(1-\Phi)\ln\left(\frac{L}{x_i}\right) + \alpha_o^{\frac{1}{2}}\right]^3 \tag{28}$$

Substituting Eq.(28) into Eq.(27) yields:

$$V_n = \frac{1}{\sqrt{\pi}}\left[Q^3(1-\Phi)^3 + Q^2(1-\Phi)^2\alpha_o^{\frac{1}{2}} + \frac{1}{2}\alpha_o Q(1-\Phi) + \frac{1}{6}\alpha_o^{\frac{3}{2}}\right] \tag{29}$$

The volume average particle volume is defined as the sum over all particles of the square of the volume divided by

the total volume; i.e.,

$$V_v = \frac{\sum n_i v_i^2}{\sum n_i v_i} \tag{30}$$

Generalizing Eq.(30) for the continuous distribution of particles leaving the chamber and using Eq.(27) yields:

$$V_v = \frac{\int_o^L n_o \left[v_i(x_i,L)\right]^2 dx_i}{\int_o^L n_o v_i(x_i,L) dx_i}$$

$$= \frac{\int_o^L \left[v_i(x_i,L)\right]^2 dx_i}{LV_n} \tag{31}$$

Combining Eqs.(28) and (31) gives the expression for V_v,

$$V_v = \frac{20}{\sqrt{\pi}} Q^3(1-\Phi)^3 + \left(\frac{1}{\pi V_n}\right)\left[\frac{5}{6}Q^2(1-\Phi)^2\alpha_o^2 + \frac{1}{6}Q(1-\Phi)\alpha_o^{\frac{5}{2}} + \frac{1}{36}\alpha_o^3\right] \tag{32}$$

The frequency function $f\left[v_i(x_i,L)\right]$ for the particle size distribution is defined such that the probability of finding a particle between particle volumes v_1 and v_2 is given by $\int_{v_1}^{v_2} f dv$. The frequency function has certain properties; i.e., $\int_o^\infty f dv \equiv 1$ and frequency function has positive values. Fein defines the distribution function $F\left[v_i(x_i,L)\right]$ as the total volume of all particles of volume less than $v_i(x_i,L)$ which passes the position

x=L per second. In mathematic expression,

$$F\left[v_i(x_i,L)\right] = \int_{x_1}^{L} n_o v_i(x_i,L)dx \qquad (33)$$

Now, from the definition of the frequency function f(v), the volume of all particles of volume between $v_1 = v - \frac{dv}{2}$ and $v_2 = v + \frac{dv}{2}$ is given by $n_o L v f(v)dv$, and thus $F\left[v_i(x_i,L)\right]$ also is given by:

$$F(V) = \int_{v_o}^{v} n_o L v f(v)dv \qquad (34)$$

where v is a function of both x_i and L. Differentiating Eq.(34) with respect to v and rearranging yields the relation between the frequency function f(v) and the distribution function F(v),

$$f(v) = \frac{F'(v)}{n_o L v} \qquad (35)$$

By differentiating Eq.(33) with respect to x_i,

$$\frac{dF(v)}{dx_i} = - n_o v \qquad (36)$$

By differentiating Eq.(28) with respect to x_i, we obtain:

$$\frac{dv}{dx_i} = - \frac{1}{2\sqrt{\pi}\, x_i}\left[Q^3(1-\Phi)^3\left(\ln\frac{L}{x_i}\right)^2 + 2Q^2(1-\Phi)^2\alpha_o^{\frac{1}{2}} \ln\frac{L}{x_i} + \alpha_o Q(1-\Phi)\right] \qquad (37)$$

By squaring Eq.(23) and rearranging, we obtain:

$$\alpha_o^{\frac{1}{2}} = \alpha^{\frac{1}{2}} - Q(1-\Phi)\ln \frac{L}{x_i} \tag{38}$$

By combining Eqs.(37) and (38), α_o is eliminated,

$$\frac{dv}{dx_i} = - \frac{Q(1-\Phi)}{2\sqrt{\pi}} \frac{\alpha}{x_i} \tag{39}$$

From the chain rule,

$$F'(v) = \frac{dF(v)}{dx_i} \frac{dx_i}{dv} \tag{40}$$

Substituting Eqs.(36) and (39) into Eq.(40) and substituting the resulting expression for F'(v) into Eq.(35) yields:

$$f(v) = \frac{2\sqrt{\pi}}{Q(1-\Phi)\alpha} \frac{x_i}{L} \tag{41}$$

From Eq.(28), we obtain:

$$\frac{x_i}{L} = \exp.\left[\frac{\alpha_o^{\frac{1}{2}} - (6\sqrt{\pi}\, v_i)^{\frac{1}{3}}}{Q(1-\Phi)} \right] \tag{42}$$

If Eq.(10) is solved for α_o,

$$\alpha_o = (6v_o)^{\frac{2}{3}} \pi^{\frac{1}{3}} \tag{43}$$

Finally, substituting Eq.(43) into Eq.(42) and substituting the resulting equation into Eq.(41), the final form of the frequency function is obtained:

$$f(v) = \frac{2\pi^{\frac{1}{6}}}{Q(1-\Phi)(6v)^{\frac{2}{3}}} \exp.\left[\frac{-\pi^{\frac{1}{6}}\left\{(6v)^{\frac{1}{3}} - (6v_o)^{\frac{1}{3}}\right\}}{Q(1-\Phi)}\right] \qquad (44)$$

If it is assumed that the volume of a nucleus (v_o) is very small compared to the number average particle volume (V_n), the equations for V_n, V_v, and f(v) can be greatly simplified. When v_o approaches zero in Eq.(10), α_o becomes zero to satisfy the equation. Under this assumption, $V_n \gg V_o$, the terms containing α_o in Eqs.(29) and (32) can be neglected to give:

$$V_n = \frac{1}{\sqrt{\pi}} Q^3(1-\Phi)^3 \qquad (45)$$

$$V_v = \frac{20}{\sqrt{\pi}} Q^3(1-\Phi)^3 \qquad (46)$$

If Eq.(45) is solved for $Q(1-\Phi)$ and the result is substituted into Eq.(44), f(v) becomes:

$$F(v) = \frac{2}{V_n^{\frac{1}{3}}(6v)^{\frac{2}{3}}} \exp.\left[-\left(\frac{6v}{V_n}\right)^{\frac{1}{3}}\right] \qquad (47)$$

It can be seen that, when $v_o \ll V_n$, the ratio of V_v to V_n is 20. In the limit as v_o gets very large, $\frac{V_v}{V_n}$ approaches unity.

C. The Results of Fein's Surface-Burning Model

The frequency function f(v) in Eq.(47) is normalized,

that is, $\int_c^\infty f(v)dv \equiv 1$. The frequency function for the partical size distribution now can be expressed for the given value of V_n.

Substituting the experimental number average particle volume, V_n, into Eq.(47), Fein obtained the theoretical frequency functions as follow:

$$f(v) = \frac{0.663 \times 10^4}{v^{\frac{2}{3}}} \exp.\left[-2 \times 10^4 \times v^{\frac{1}{3}}\right],$$

$$V_n = 0.75 \times 10^{-12} cm^3 \tag{48}$$

$$f(v) = \frac{1.99 \times 10^4}{v^{\frac{2}{3}}} \exp.\left[-6.02 \times 10^4 \times v^{\frac{1}{3}}\right],$$

$$V_n = 0.0274 \times 10^{-12} cm^3 \tag{49}$$

The values of V_n in Eqs.(48) and (49) are measured at the chamber pressures of 34 and 10.2 atm, respectively, in Fein's experiments. When the volume average particle volume (or the weight average particle volume) is $V_v = 0.523 \times 10^{-18}$ cm^3, or $V_n = \frac{1}{20} V_v = 2.615 \times 10^{-20}$ cm^3, the corresponding frequency function according to Fein's system model is:

$$f(v) = \frac{2.05 \times 10^6}{v^{\frac{2}{3}}} \exp.\left[-6.15 \times 10^6 v^{\frac{1}{3}}\right] \tag{50}$$

The above exemplified value for V_v is equivalent to 100 $\mathring{A}$ diameter particle size which is desired for colloid thrustor. Eqs.(48) and (49) are plotted in Figures (19)

and (20). The individual points on the graphs are Fein's experimental results. Comparison of Fein's analysis with his experimental results shows excellent agreement between the theory and experiments. Samples of particles collected by Sehgal (reference 32) were sent to Fein. In Sehgal's work, the propellant composing of 12% aluminum, 19% polyurethane binder, and 69% ammonium perchlorate was fired into a stainless steel collecting tank at the ambient pressures of 34 and 10.2 atm respectively. Fein dispersed and photographed these particles through an electron microscope and determined particle-size distributions by counting the particles in the photomicrographs. This fact justifies those five assumptions made early by Fein. If Eq.(25) is multiplied by Q,

$$\left(\frac{K_1}{K_2}\right)\left(\frac{\Phi}{n_o}\right) = 2Q^3(1-\Phi)^3 + 2Q^2(1-\Phi)^2\alpha_o^{\frac{1}{2}} + Q(1-\Phi)\alpha_o \qquad (51)$$

where

$$K_1 = \frac{\sqrt{\pi}\,\delta_M dP}{2\rho_N \rho_p rRT} = \frac{Q}{\gamma} \qquad (52)$$

$$K_2 = \frac{1}{4\pi}\left(\frac{P}{N\rho_p rRT}\right)^2 = \frac{B}{\gamma} \qquad (53)$$

$$\frac{K_1}{K_2} = \left(\frac{2\pi^{\frac{3}{2}}\delta_{MN}\rho_p rRT}{\rho_p}\right)d = \frac{Q}{B} \qquad (54)$$

Dividing Eq.(51) by $2\sqrt{\pi}$ and then add to it the quantity which is the result of Eq.(10), i.e., $v_o = \left(\frac{1}{6\sqrt{\pi}}\right)\alpha_o^{\frac{3}{2}}$,

the result is then equal to V_n as given by Eq.(29). Therefore, we have,

$$V_n = \left(\frac{1}{2\sqrt{\pi}}\right)\left(\frac{K_1}{K_2}\right)\left(\frac{\Phi}{n_o}\right) + v_o$$

$$= \left(\frac{1}{2\sqrt{\pi}}\right)\left(\frac{K_1}{K_2}\right)\left(\frac{\Phi}{n_o}\right) \quad , \text{ when } \quad v_o \ll V_n \qquad (55)$$

The values for nucleation rate (n_o) computed by Fein are 2.35×10^{12} and 4.48×10^{13} nuclei/sec/cm at chamber pressures of 34 and 10.2 atm, respectively. The various constants used by Fein in his computations are listed in Table VI. n_o appears to be a strong function of pressure with n_o decreasing as pressure increases. From this fact, Fein concluded that nucleation process is not homogeneous, because homogeneous nucleation rates generally increase with increasing concentration of the condensable species, and concentration increases with increasing pressure. This conclusion that the nucleation is not homogeneous is already indicated by Courtney (reference 25) and Gordon (reference 26). In Fein's analysis, the frequency function for the particle-size distribution is independent of the chamber length (L), but dependent upon nucleation rate (n_o).

D. Vapor-Phase Burning Model

In Fein's model, aluminum burns at high pressure (for example 34, 10.2 atm), and therefore it does not burn a vapor phase. As a result, it is expected that this

surface burning mechanism of aluminum directly implies a wide particle-size distribution. Vapor-phase burning of aluminum should produce a much narrower particle-size distribution because of rapid nucleation rate by virtue of a higher degree of supersaturation (reference 2). A vapor-phase burning model expected to produce a narrower particle-size distribution is shown in Figure 24. A central jet of aluminum vapor is enclosed in an annulus of oxygen to produce a flame. This model, in contrast to Fein's, will therefore have a linearly diminishing aluminum vapor pressure. The oxygen pressure can be assumed constant throughout the length of chamber. This new model changes the Fein's assumption (3). New assumption satisfying new model is that the velocity of combustion product is proportional to the flow rate of aluminum and oxygen vapor (or proportional to the consumption rate of aluminum) (g/sec), and the velocity is expressed by Eq.(56).

$$u = N\dot{m} \left(\frac{RT}{P}\right) \frac{1}{A} \tag{56}$$

where u = velocity of combustion products, cm/sec

N = moles of combustion products produced from the burning of 1 g aluminum, moles/g

$\dot{m}$ = consumption rate of aluminum, g/sec.

A = cross sectional area of inside cylinder in Figure 24, cm^2

R = gas constant, 82.057 $(cm^3)(atm)/(^oK)(g\text{-}mole)$

T = absolute temperature, ^oK

P = pressure, atm

The rest of Fein's assumptions are suitable for the above new model for which a new size distribution will be derived. By using the simple definition of linear velocity

$u = \frac{dx}{d\theta}$ in Eq.(56), we obtain:

$$d\theta = \frac{AP}{\dot{N}_m RT} dx \quad . \tag{57}$$

Changing independent variable from time (θ) to distance (x) by substituting Eq.(57) into Eq.(3) yields:

$$dv = \left[\gamma (C-C_e) \alpha \frac{M}{\rho} \right] \frac{AP}{\dot{N}_m RT} dx \tag{58}$$

Combination of Eqs.(11) and (58) eliminates dv and reduces Eq.(58) to Eq.(59) after performing integration between the limits, (α_o, x_i) to (α, L).

$$\alpha^{\frac{1}{2}} = 2\sqrt{\pi} \left[\gamma (C-C_e) \frac{M}{\rho} \right] \frac{AP}{\dot{N}_m RT} (L-x_i) + \alpha_o^{\frac{1}{2}} \tag{59}$$

As previously described in Section (B), $v_o \ll V_n$ and therefore α_o becomes zero as v_o approaches zero according to Eq.(10). Eq.(59) can now be reduced to Eq.(60).

$$\alpha^{\frac{1}{2}} = 2\sqrt{\pi}\left[\gamma(C-C_e)\frac{M}{\rho}\right]\frac{AP}{NnRT}(L-x_i),\quad v_o \ll V_n$$

$$= Q'(L-x_i) \tag{60}$$

where $$Q' = 2\sqrt{\pi}\left[\gamma(C-C_e)\frac{M}{\rho}\right]\frac{AP}{NnRT} \tag{61}$$

Squaring Eq.(60), we obtain:

$$\alpha = (Q')^2(L-x_i)^2 \tag{62}$$

Substituting Eq.(62) into Eq.(10), we obtain:

$$v = \frac{1}{6\sqrt{\pi}}(Q')^3(L-x_i)^3 \tag{63}$$

We can redefine the Eq.(27), assuming the constant number of nuclei in the chamber, $V_n = \int_o^L v_i dx_i$. Substituting Eq.(63) into the redefined V_n above and performing integration,

$$V_n = \frac{(Q')^3 L^4}{24\sqrt{\pi}} \tag{64}$$

Differentiating Eq.(63) with respect to x_i, and substituting the value of $(L-x_i)^2$ of Eq.(62) into the resultant equation,

$$\frac{dv}{dx_i} = -\frac{Q'\alpha}{2\sqrt{\pi}} \tag{65}$$

Substituting Eqs.(36) and (65) into Eq.(40), we obtain:

$$F'(v) = \frac{2n_o v\sqrt{\pi}}{Q'\alpha} \tag{66}$$

Substituting Eq.(66) into Eq.(35),

$$f(v) = \frac{2\sqrt{\pi}}{LQ'\alpha} \tag{67}$$

Substituting Eq.(62) into Eq.(67),

$$f(v) = \frac{2\sqrt{\pi}}{L(Q')^3(L-x_i)^2} \tag{68}$$

Substituting the value for $(L-x_i)^2$ of Eq.(63) and subsequently substituting the value for Q' of Eq.(64), we obtain the final form of $f(v)$ providing that the length of chamber L is unity:

$$f(v) = 0.21\ V_n^{-\frac{1}{3}}\ v^{-\frac{2}{3}} \tag{69}$$

Since the constant term in Eq.(69) will be normalized later, the length of chamber (L) can be chosen arbitrarily. A particle-mass distribution function un-normalized for the new model is obtained using $V_n = 2.615 \times 10^{-20} cm^3$ and expressing Eq.(69) in terms of particle mass (m).

$$f(m) = 17.9 \times 10^5\ m^{-\frac{2}{3}} \tag{70}$$

Normalizing Eq.(70) with the maximum particle mass ($\cong 10^{-12}$g); i.e., $\int_0^{m(max.)} f(m)\ dm \equiv 1$, the normalized equation for f(m) is obtained:

$$f(m) = 3.34 \times 10^3\ m^{-\frac{2}{3}} \tag{71}$$

The maximum particle mass is apparently not infinity, and therefore the definition of particle-mass distribution

function, $\int_0^{\infty} f(m)dm \equiv 1$, should be modified to $\int_0^{m(max.)} f(m)dm \equiv 1$. Numberical calculations for the thrustor efficiency shows that an arbitrary choice of the maximum particle mass (not infinity) yields the same result of thrustor efficiency.

E. Colloid Thrustor Efficiencies for Surface-Burning and Vapor-Phase Burning Models

It is required to know the particle-mass distribution in order to predict the thrustor efficiency. The colloid thrustor with narrower particle-size distribution has higher efficiency than that with wider size distribution. The effect of particle-size distribution on colloidal-particle-thrustor efficiency is illustrated by Mickelsen and Kaufman (reference 31) by the following expression;

$$\eta = \eta_u \frac{\left(\int_0^{\infty} \sqrt{m}\, f(m)dm\right)^2}{\left(1 + \frac{\sum P_l}{J\Phi_{net}}\right)\int_0^{\infty} mf(m)dm} \qquad (72)$$

where

η = thrustor efficiency

η_u = propellant-utilization efficiency

$f(m)$ = particle-mass distribution function, g^{-1}

m = particle mass, g

$\sum P_l$ = total power loss, w

J = ion current density, amp./sq.m

Φ_{net} = net accelerating voltage, volt.

For the ideal colloid thrustor, the net power loss $\sum P_l$ is assumed zero, and thus the ideal thrustor efficiency can be simply expressed by Eq.(73) providing that propellant-utilization efficiency η_u is 100%.

$$\eta = \frac{\left(\int_0^\infty \sqrt{m}\, f(m)dm\right)^2}{\int_0^\infty mf(m)dm} \qquad (73)$$

By changing the independent variable from particle volume (v) to particle mass (m) in Eq.(50), the particle-mass distribution function f(m) is obtained as follow:

$$f(m) = 5.16 \times 10^6 \times m^{-\frac{2}{3}} \exp.\left[-3.89 \times 10^6\, m^{\frac{1}{3}}\right] \qquad (74)$$

Eq.(74) is renormalized into Eq.(75) by the use of normalization factor (=3.98).

$$f(m) = 1.3 \times 10^6\, m^{-\frac{2}{3}} \exp.\left[-3.89 \times 10^6\, m^{\frac{1}{3}}\right] \qquad (75)$$

The quantities, f(m), $\sqrt{m}f(m)$ and mf(m) against m are shown in Figures 21,22, and 23. Finally, 30% colloid thrustor efficiency is obtained by the use of the particle-mass distribution function in Eq.(75) which is a result of Fein's analysis. In contrast to Fein's model, the vapor-phase burning model has 64% thrustor efficiency. This improved efficiency has been calculated by performing the integration of Eq.(73) with the use of particle-mass distribution function f(m) of Eq.(71). The quantities, f(m), $\sqrt{m}f(m)$, and mf(m) against m for the vapor-phase burning model are plotted in Figures 25, 26, and 27.

CHAPTER V

Condensation of Al_2O_3

In the combustion of aluminum, it is generally considered that the Al_2O_3 particles are growing through a very complicated chemical reaction between the surface of oxide film and the vapor phases, Al(g), AlO(g), O(g), and O_2(g). In such a heterogeneous condensation process, a variety of chemical reactions preceding condensation is rate controlling. From this view-point, the classical liquid-drop theory of homogeneous condensation developed by Frenkel (reference 27), Volmer (reference 28), and Becker and Doring (reference 29) is, therefore, not valid for the heterogeneous condensation of Al_2O_3 particles. Work in related fields, such as chemical kinetics, surface processes, and transport phenomena, is of importance to predict the condensation rate in the combustion system. However, there appears to be no quantitative development of nucleation or condensation theory in combustion systems. Furthermore, no experimental data on the condensation rate in combustion systems has been reported in the open literature. At present, the rate of condensation in a combustion system is only of academic interest. Finally, it should be mentioned that the determination of Al_2O_3 particle formation efficiency has to rely upon the experiment.

CHAPTER VI

CONCLUSIONS

Aluminum wire or aluminum particles (smaller than about 50 micron) can burn in a vapor-phase when the combustion chamber pressure is maintained below 500 mmHg and high mole fraction of O_2 is maintained throughout the combustion process (region 3 in Figure 4). The effect of net rate of heat loss from the flame on the vapor-phase burning criterion has been discussed, because Glassman's criterion for vapor-phase burning is a necessary but not sufficient condition. Therefore, for the vapor-phase combustion of aluminum, it is not required to vaporize aluminum prior to chemical reaction with oxygen. Al wire burning seems to be very promising because no extra heat is required to vaporize aluminum, and the control of aluminum wire burning is much easier than the aluminum powder in the laboratory situation.

The vapor-phase burning is sought here in a hope to obtain a uniform size of small colloid particles (10-100 Angstrom diameter) which may be desirable in colloid propulsion systems. The ignition temperature of aluminum coincides with the melting point of Al_2O_3 (2318°K). This is because the melting of the aluminum oxide layer causes the increase in the chemical reaction rate and leads to the ignition of aluminum. The adiabatic flame temperature calculated in Section E, Chapter II, 3980°K is comparable

with 3908°K in Table II which is calculated by Fassell (reference 12). This discrepancy probably came from the use of different sources of thermodynamic data. The actual flame temperature is lower than the adiabatic flame temperature by virtue of the radiation loss from the flame. The rate of radiation heat loss is a function of various parameters, such as the particle size, chamber pressure, wall reflectivity, the particle concentration, and the chamber wall temperature. The mathematical evaluation of radiation energy loss from the flame was unable to be made because of the unknown nature of scattering and absorption of small Al_2O_3 particles in the flame. In terms of the number average particle volume, V_n, the normalized frequency function f(v) for the distribution of particle volume v is derived by Fein in Eq.(47). Fein's conclusions from his analysis of particle-size distributions are: (1) the particle-size distribution is independent of chamber length (L) and depends upon the nucleation rate (n_o), (2) the nucleation process is not homogeneous. The 30% thrustor efficiency is obtained by applying Fein's analysis to the case in which weight average particle volume $V_v = 0.523 \times 10^{-18}$ cm^3 or $V_n = \frac{1}{20}V_v = 2.615 \times 10^{-20}$ cm^3. The effect of changing V_v on the thrustor efficiency is proved to be negligible. An improved thrustor efficiency of 64%, in contrast to Fein's model, is obtained from the vapor-phase burning model (see

Figure 24). The explanation for this improved efficiency can be found from the fact that a vapor-phase flame produces a uniform size of colloid particles and thus the new model has higher efficiency.

BIBLIOGRAPHY

1. Goldin, D.S., and Kritek, G.L., An Analysis of Particle-Formation Efficiency in a Colloid Thrustor. AIAA Paper No. 66-253, March 1966

2. Courtney, W.G., Colloid Propulsion Using Chemically-Formed Particles, AIAA paper No. 66-254

3. Mickelsen, W.R., Future Trends in Electric Propulsion. AIAA paper No. 66-595, June 1966

4. Grosse, A.V., and Conway, J.B., "Combustion of Metals in Oxygen", Industrial Engineering Chemistry 50, pp. 663-672 (1958)

5. McBride, B.J., Heimel, S., Ehlers, J.G., and Gordon, S., Thermodynamic Properties to 6000°K for 210 Substances Involving the First 18 Elements. NASA SP-3001, National Aeronautics and Space Administration, Lewis Research Center, Cleveland, Ohio. 1963

6. Dow Chemical Company, JANAF Thermochemical Data, Interim Tables, December 1960

7. Kubaschewski, O., and Evans, E., Metallurgical Thermochemistry, Pergamon Press Ltd., 1958

8. Glassman, I., "Metal Combustion Processes", American Rocket Society preprint 938-59, November 1959

9. Glassman, I., "Combustion of Metals, Physical Considerations", Summerfield, M.(ed.), Solid Propellant Rocket Research, Academic Press, New York, 1960, pp. 253-258

10. Brzustowski, T.A., Vapor-Phase Diffusion Flames in Combustion of Mg and Al. ph.D. Thesis, Department of Aeronautical Engineering of Princeton University, New Jersey, 1963

11. Byrne Jr., W.M., "Radiant Heat Transfer to an Enclosure from Two-Phase Flows", Journal of Spacecraft and Rockets, vol. 3, No. 6, June 1966, pp. 919-924

12. Fassell, W.M., Papp, C.A., Hildenbrand, D.L., and Sernka, R.P., "The Experimental Nature of the Combustion of Metallic Powders", Summerfield, M.(ed.), Solid Propellant Rocket Research, Academic Press, New York, 1960, pp. 259-269

13. Rautenberg Jr., J.H., and Johnson, P.D., "Light Production in the Aluminum-Oxygen Reaction", Journal of American Optical Society, 50, pp. 602-606, June 1960

14. Reynolds, W.G., "Investigation of Ignition Temperatures of Solid Metals", NASA TN D-182, October 1959

15. Pearse, R.W. B., and Gaydon, A.G., Identification of Molecular Spectra, Wiley, 1950

16. Gordon, D.A., "Combustion Characteristics of Metal Particles", Progress in Astronautics and Rocketry, Vol. I, Solid Propellant Rocket Research, Academic Press, 1960

17. Harrison, P.L., and Yoffee, A.D., "The Burning of Metals", Proceedings Series A, Royal Society of Londc 261, May 1961, pp. 357

18. Kirschfeld, L., "Über die Verbrennungsgeschwindigkeit von Leichtmetalldrähten in Sanerstoff", Metall 14, 213-219 (1960), also "Über die Verbrennungsgeschwindigkeit von Leichtmetalldrähten in Sauerstoff hohen Drukes",Metall 15, 873-878 (1961)

19. Friedman, R., and Maček, A., "Combustion Studies of Single Aluminum Particles", Ninth Symposium (International) on Combustion, Academic Press, New York, 1963, pp. 703-712

20. Wolfhard, H.G., and Parker, W.G., "Temperature Measurements of Flames Containing Incandescent Particles", Proceedings of Physical Society (London), 62B, pp. 523-529 (1949)

21. Brewer, L., and Searcy, A.W., "The Gaseous Species of the Al-Al_2O_3 System", Journal of American Chemical Society, Vol. 73, pp. 5308-5314, 1951

22. Ackermann, R.J., Thorn, R.J., and Winslow, G.H., "Systematic Trends in Vaporization and Thermodynamic Properties of Oxides", Planetary and Space Science, Vol. 3, February 1961

23. International Critical Tables of Numerical Data, Physics, Chemistry, and Technology, National Research Council of the United States of America, Vol. V McGraw-Hill Book Company, Inc. 1933, pp. 418

24. Fein, M.L., "A Theoretical Model for Predicting Aluminum Oxide Particle Size Distributions in Rocket Exhausts", AIAA Journal, Vol. 4, No. 1, Jan. 1966, PP. 92-98

25. Courtney, W.G., "Recent Advances in Condensation and Evaporation", American Rocket Society 31, pp. 751-756 (1961)

26. Christensen, H.C., Knipe, R.H., and Gordon, A.S., "Survey of Aluminum Particle Combustion", Meeting of the Western States Section of the Combustion Institute, University of Utah, Salt Lake City, Utah, preprint 64-19 (October 1964)

27. Frenkel, J., Kinetic Theory of Liquids, New York, Dover Publications Inc., 1955

28. Volmer, M., Kinetik der phasenbildung, Edwards Bros., Ann Arbor, 1945

29. Becker, R., and Döring, W., "The Kinetic Treatment of Nucleus Formation in Supersaturated Vapors", Ann physik, Vol. 24, 1935, pp. 719

30. Brzustowski, T.A. and Glassman, I., "Spectroscopic Investigation of Metal Combustion", Aeronautical Engineering Laboratory Report No. 586, October, 1961, Guggenheim Laboratories for Aero-space Propulsion Sciences, Department of Aeronautical Engineering, Princeton University, Princeton, New Jersey.

31. Mickelsen, W.R. and Kaufman, H.R., "Status of Electrostatic Thrustors for Space Propulsion". NASA TN D-2172. May 1964.

32. Sehgal, R., "An experimental Investigation of a Gas-Particle System", TR 32-238, California Institute of Tech. Jet Propulsion Lab., Pasadena, Calif. (Mar. 16, 1962)

Figure-1 Vapor Pressures of Metals and Their Oxides

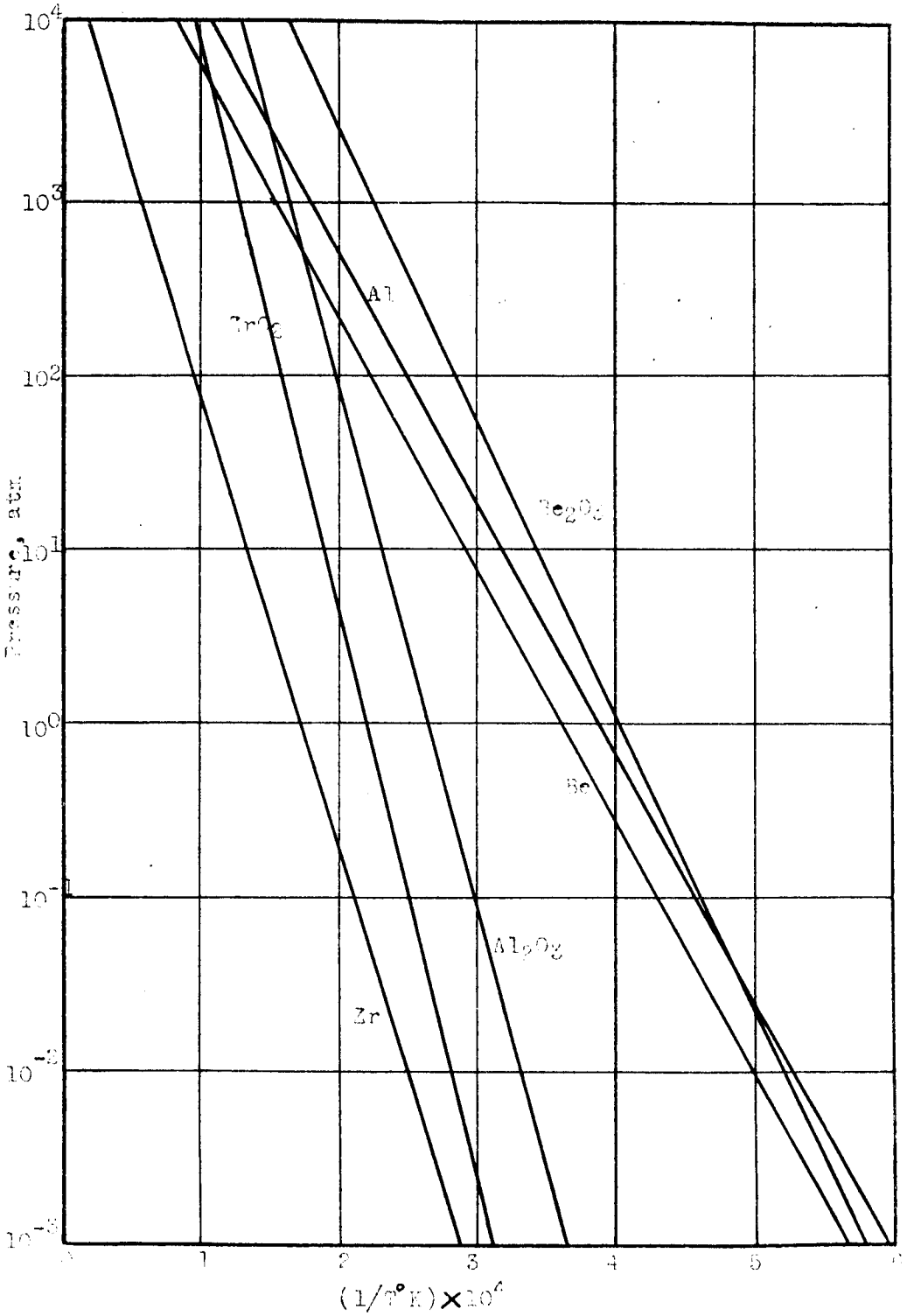

Figure-2 Q(T) versus T

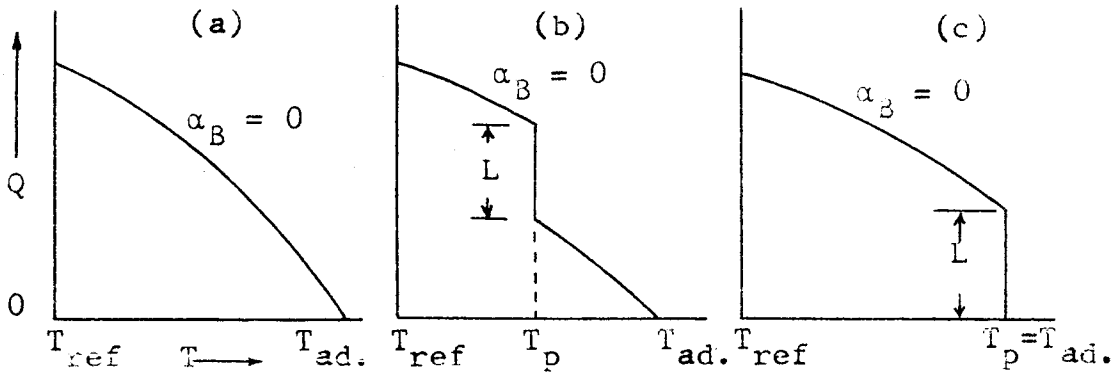

Figure-3 $q(T_B)$ and $w_f Q(T_B)$ versus T_B

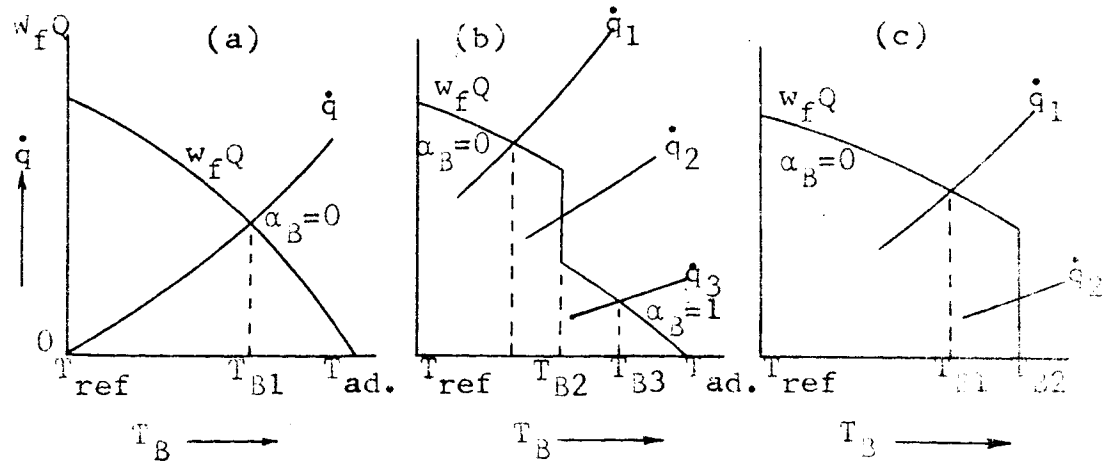

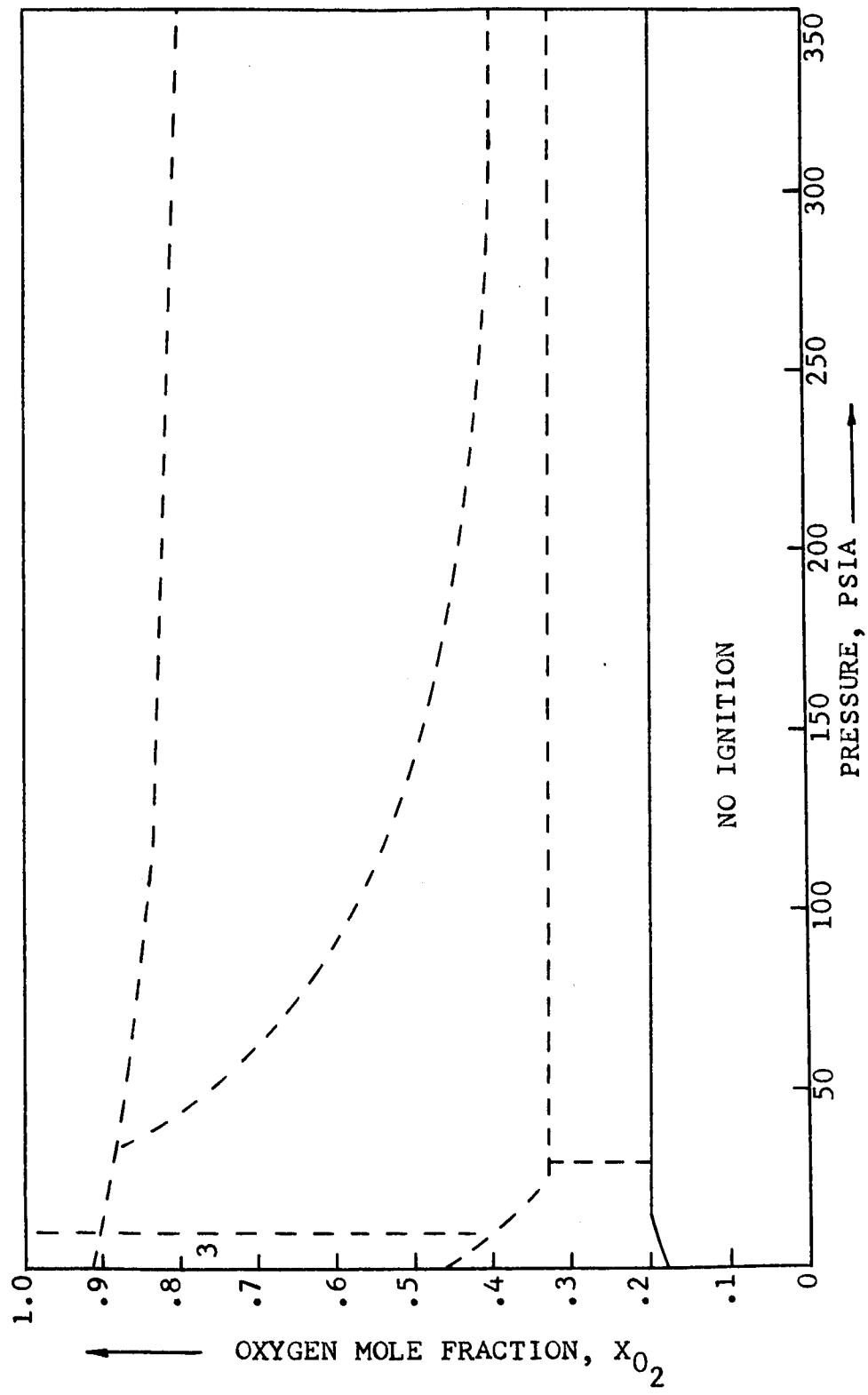

Figure-4 Combustion Mechanisms of Aluminum Wire in O_2-A Observed by Brzustowski

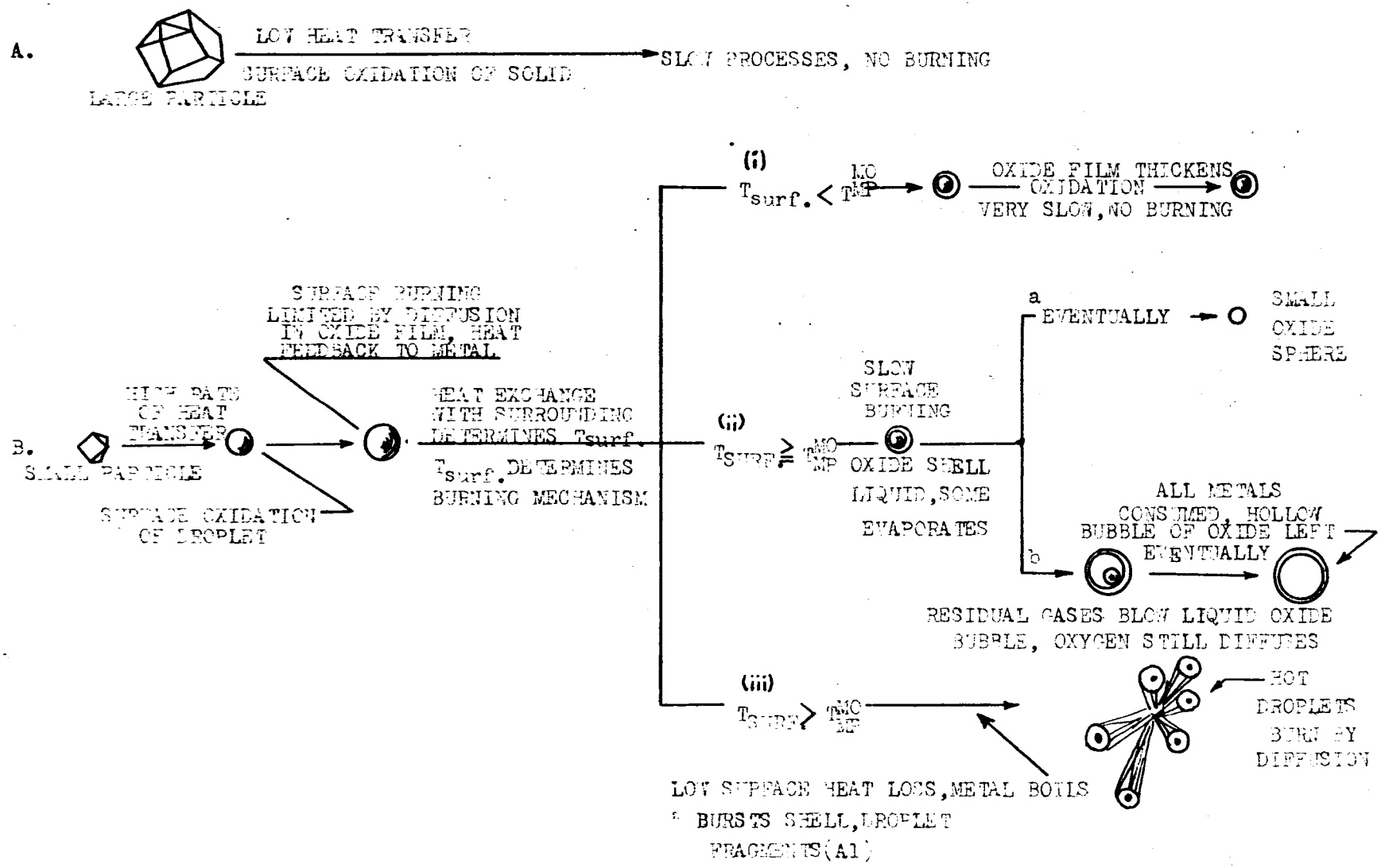

Figure-3 Burning Behavior of Al Particles

Figure-6 The Net Rate of Heat Loss (q_{loss}) and the Rate of Heat Gain from the Chemical Reaction ($q_{react.}$) versus Particle Surface Temperature

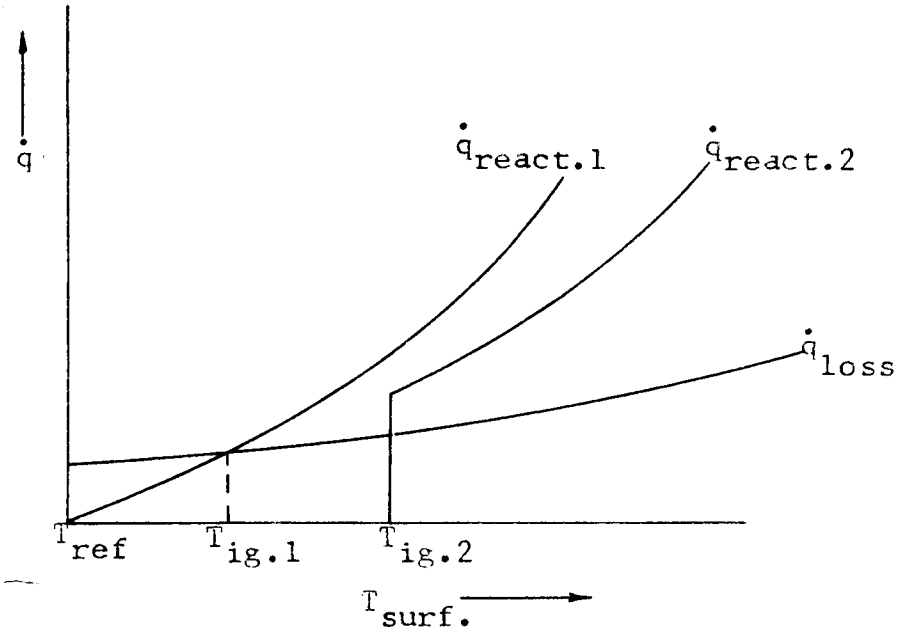

Figure-7 Minimum Ambient Temperature for Ignition of Aluminum Particles

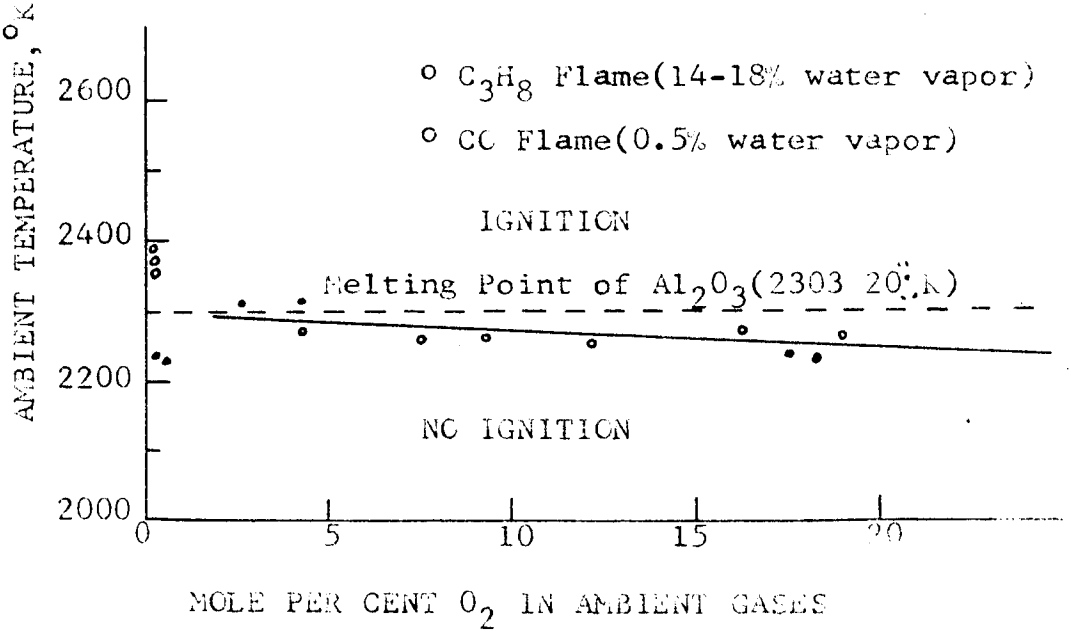

Figure-3 $LOG_{10}K_p$ versus Temperature, K

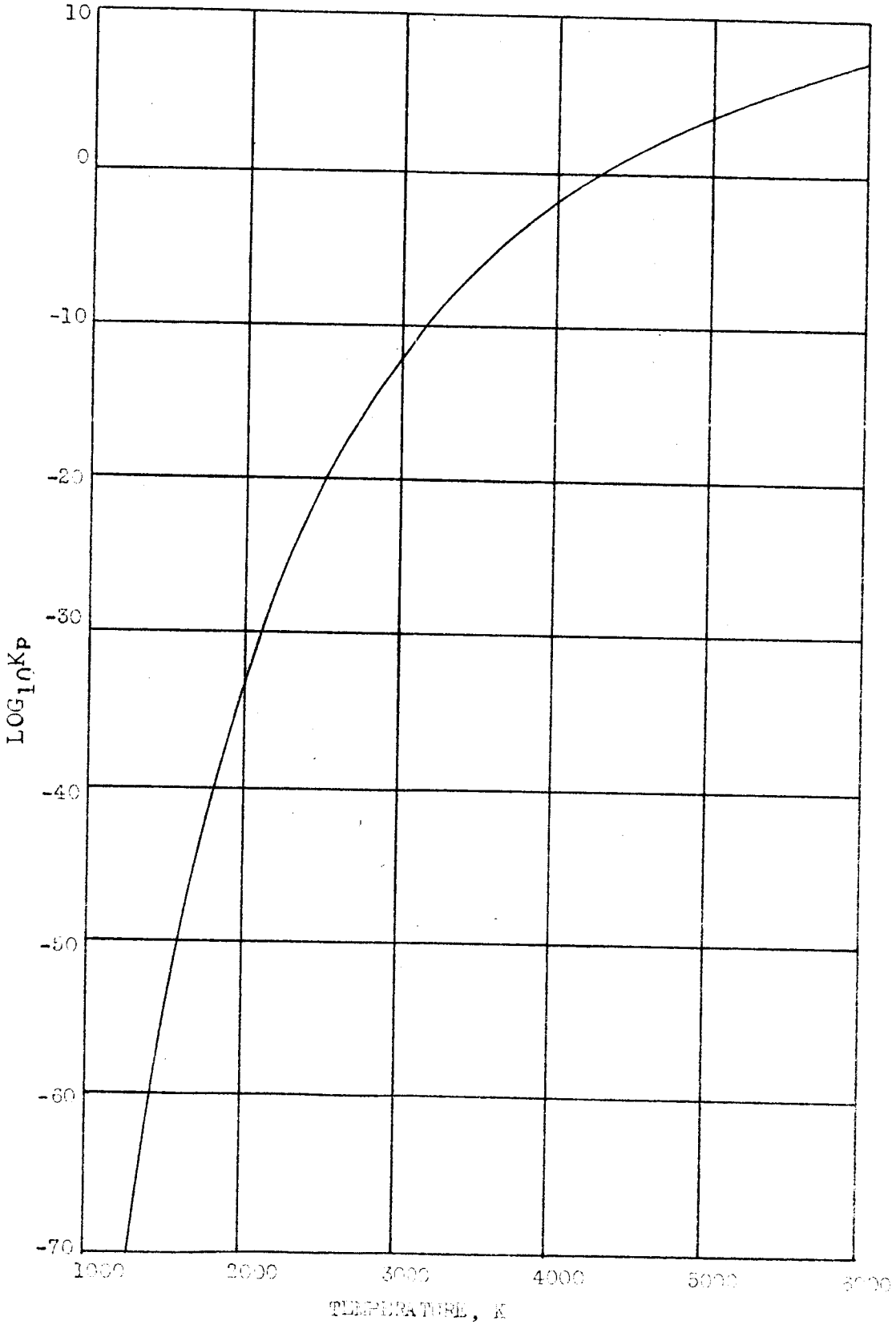

Figure-9 ΔG_T^o versus T^oK

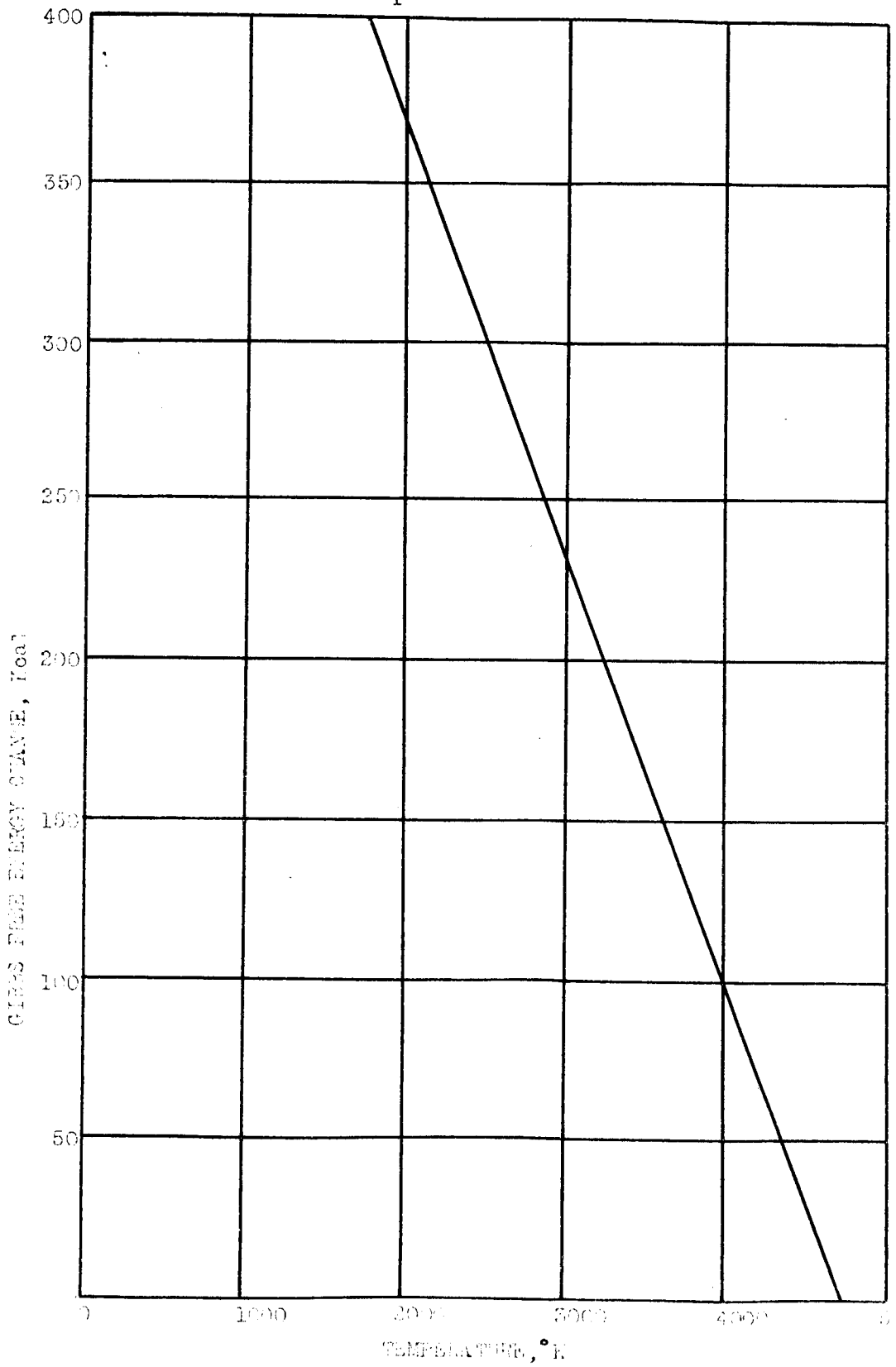

Figure-10 ΔH_T^o versus T^oK

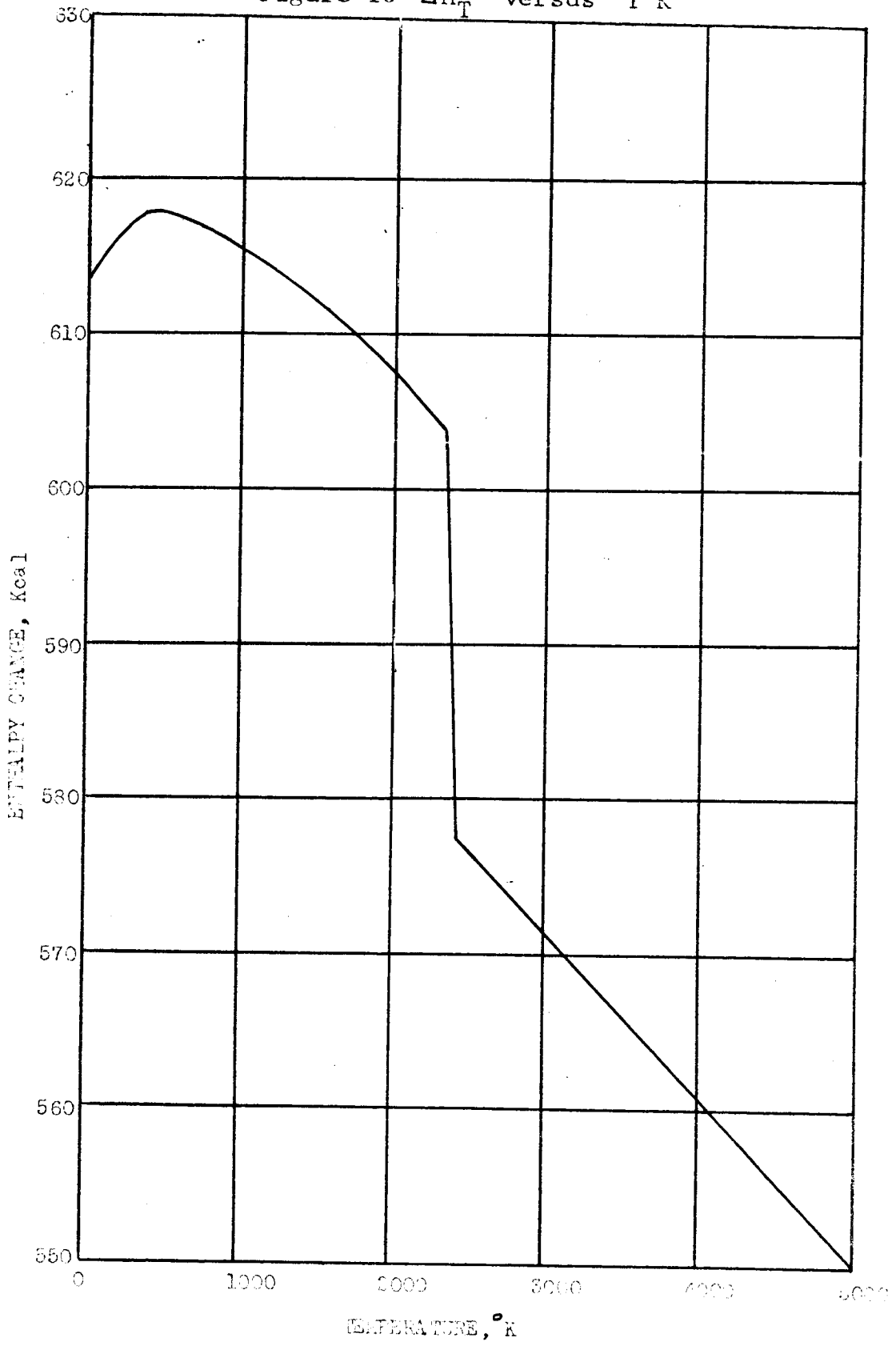

Figure-11 ΔS_T° versus T °K

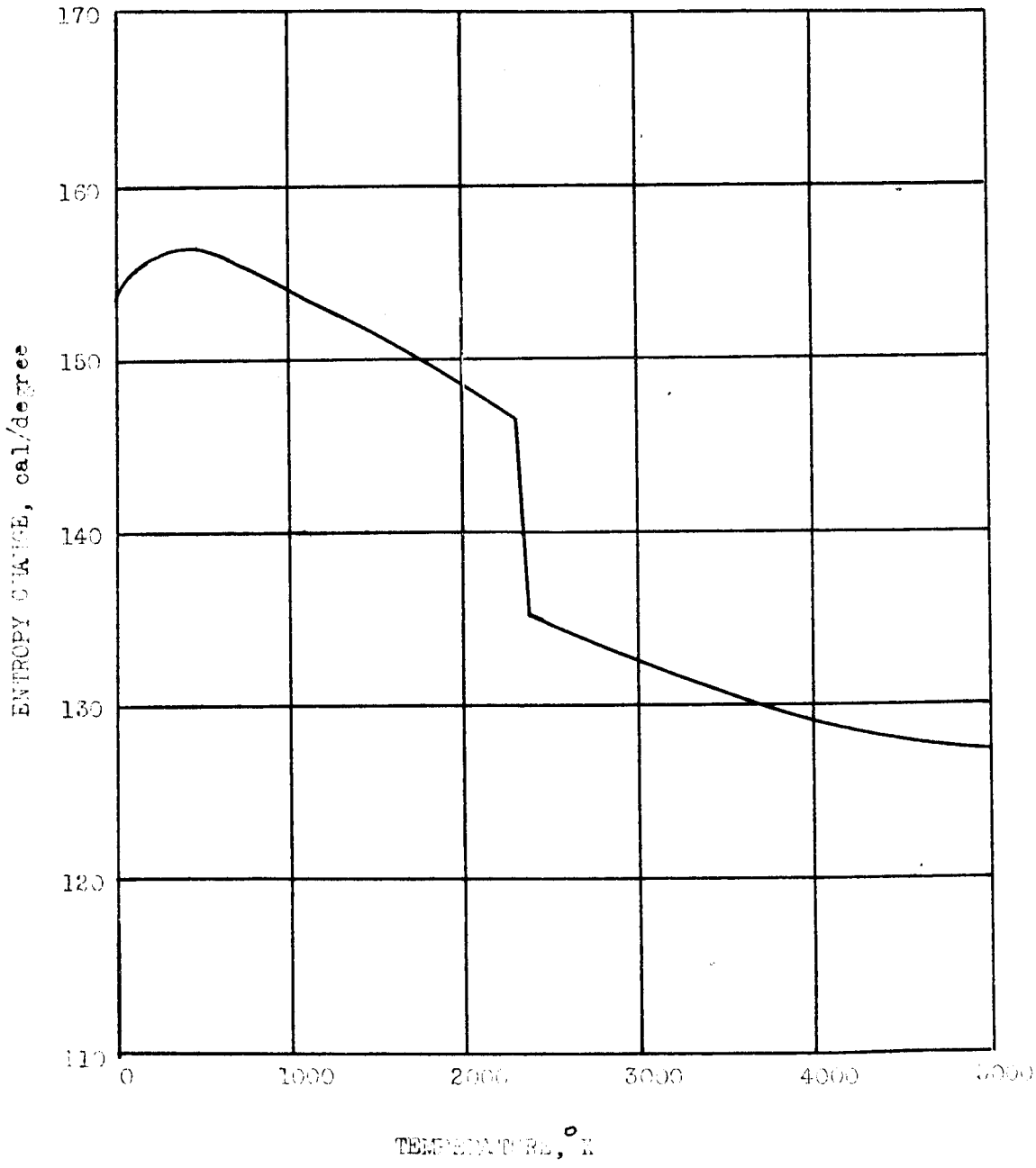

Figure-12 Particle Size Effects on Heat Flux

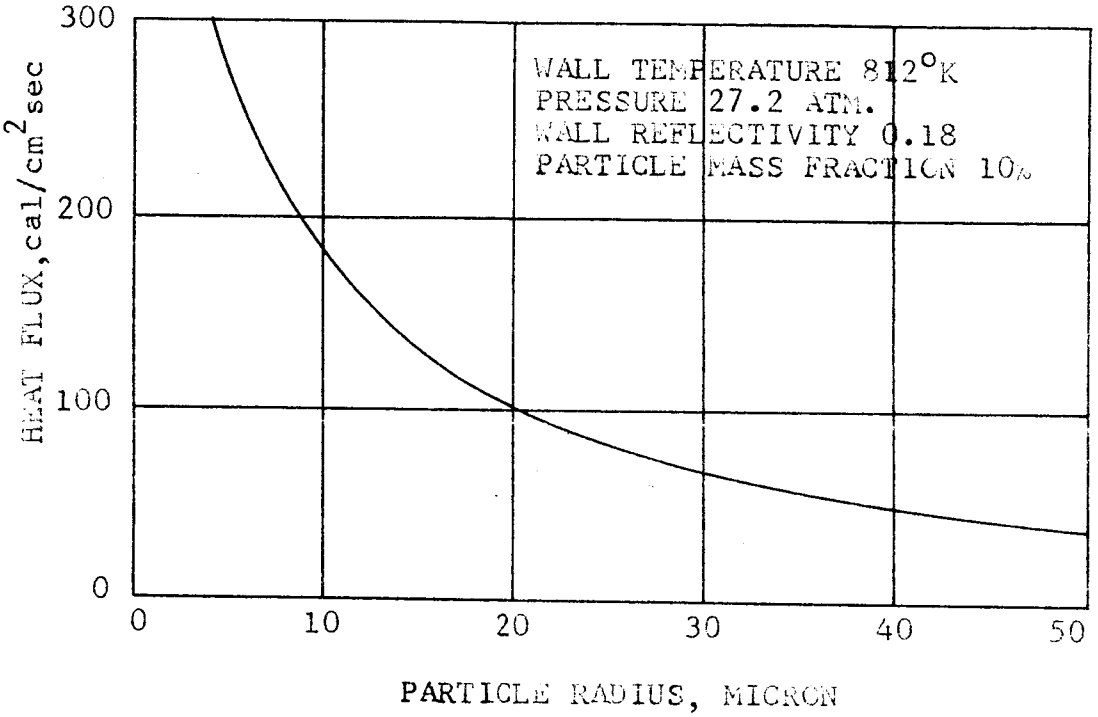

Figure-13 Chamber Pressure Effects on Heat Flux

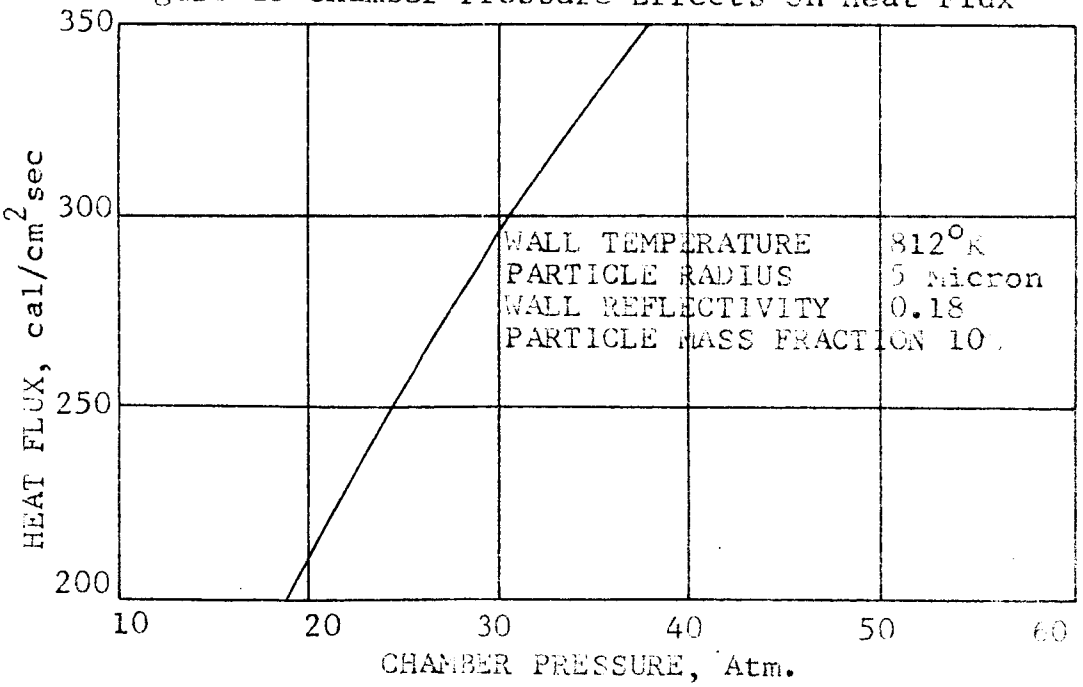

Figure-14 The Effects of Wall Reflectivity on Heat Flux

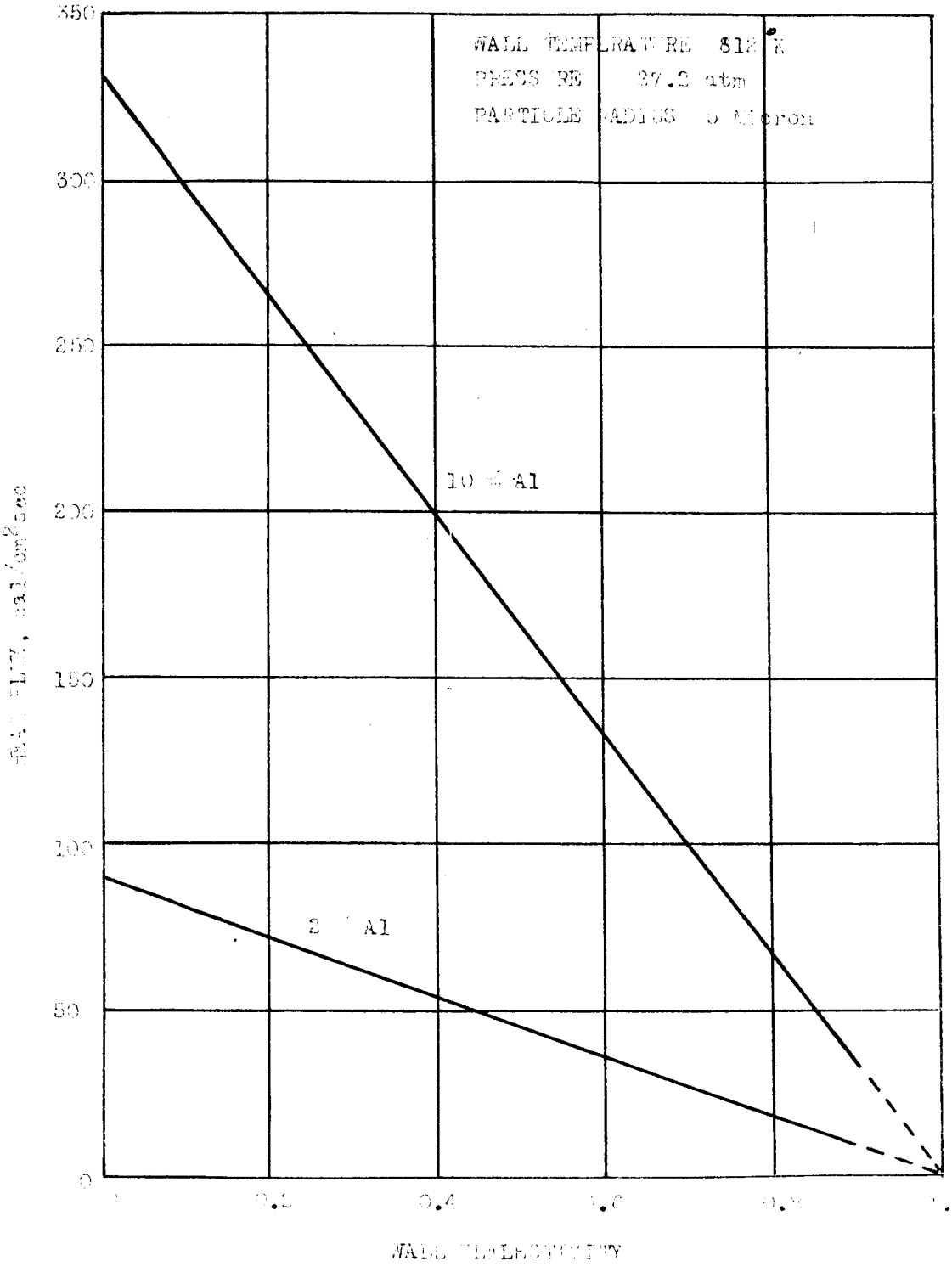

Figure-15 Wall Temperature Effects on Heat Flux

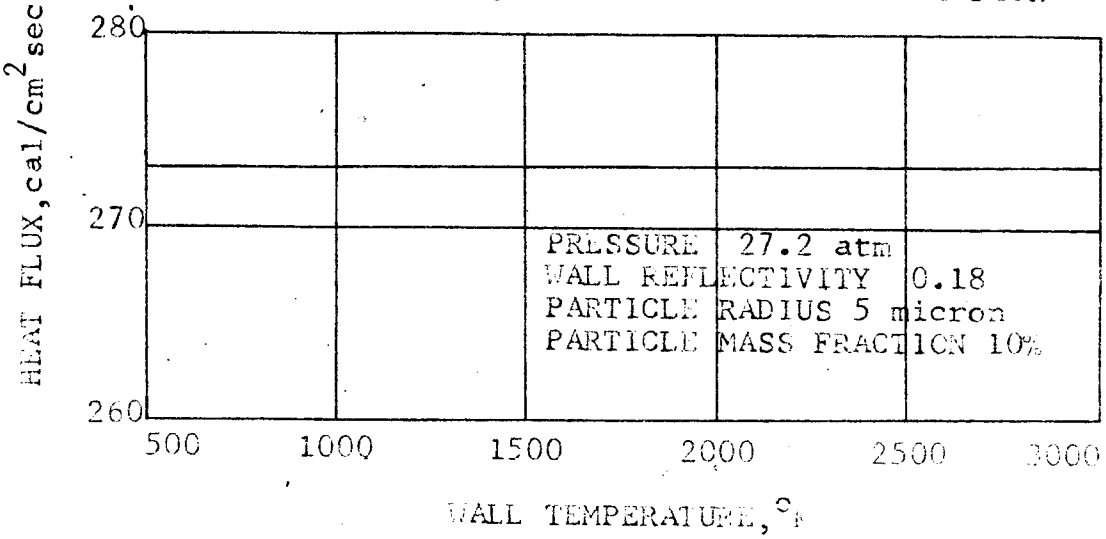

Figure-16 Apparent Emissivity versus Particle Mass Fraction

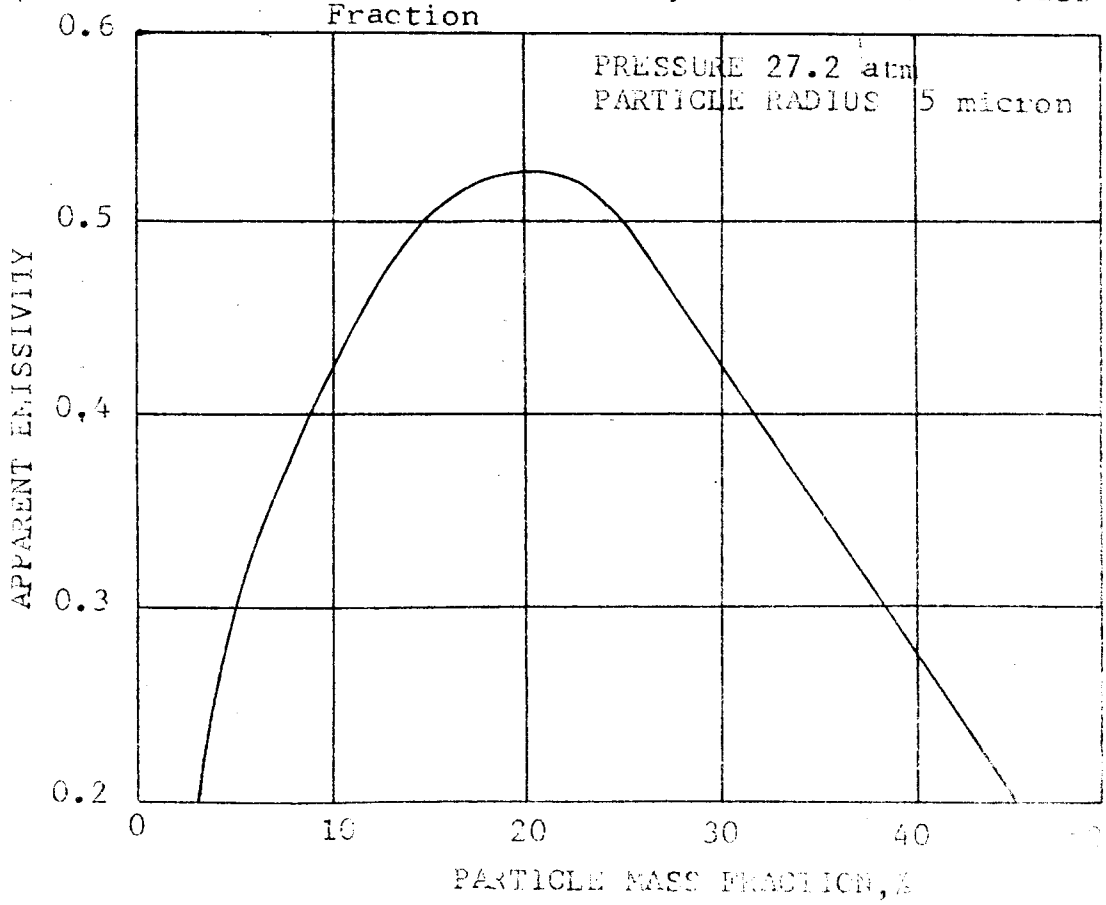

Figure-17 Schematic Diagram of a Burning Aluminum

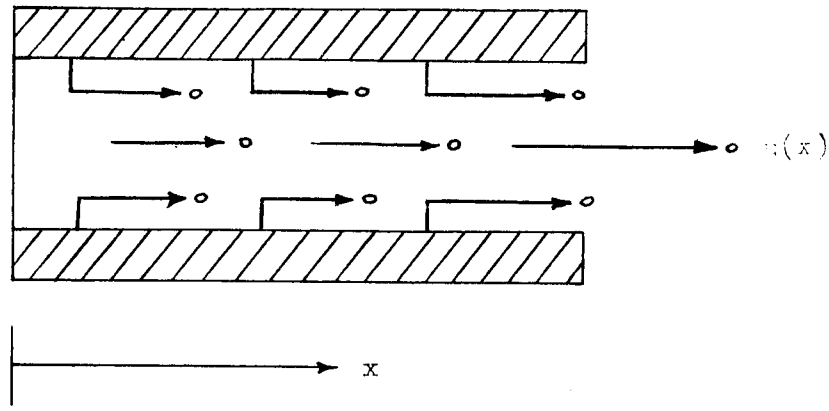

Figure-18 Differential Element of Chamber Length

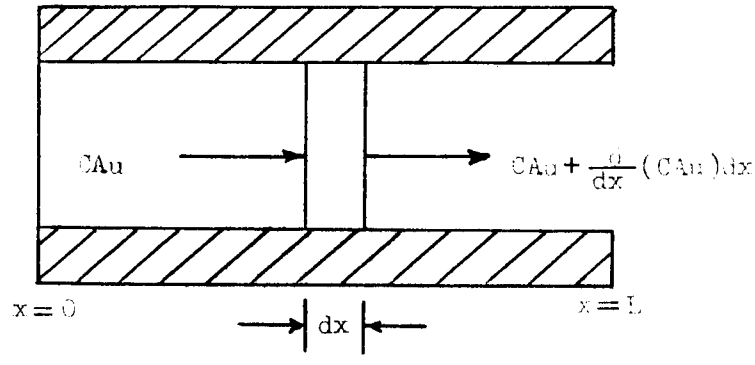

Figure-19 Theoretical Frequency Function versus Particle Volume when $V_n = 0.75 \times 10^{-12}$ cm^3

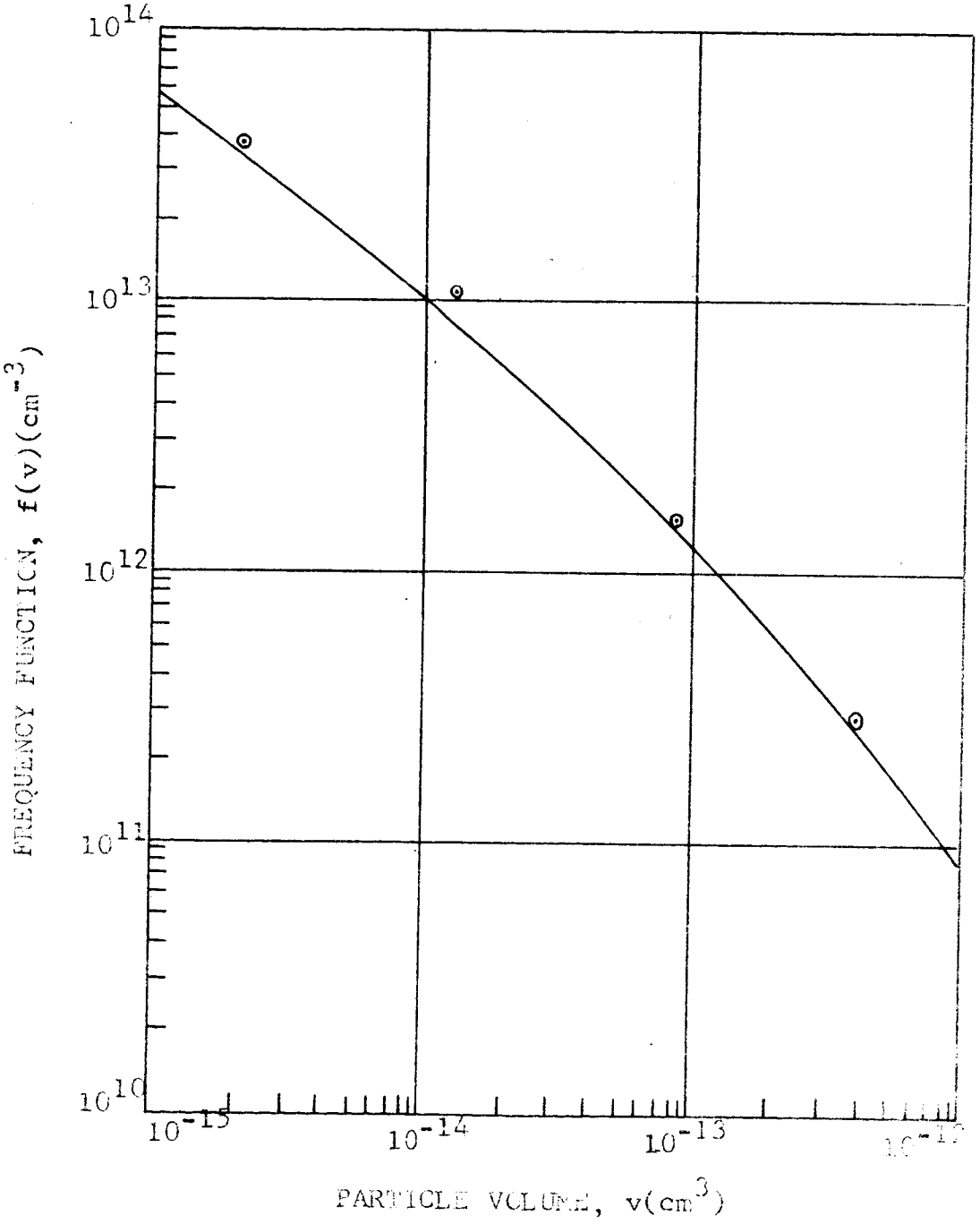

Figure-20 Theoretical Frequency Function versus Particle Volume when $V_n = 0.0274 \times 10^{-12}$ cm^3

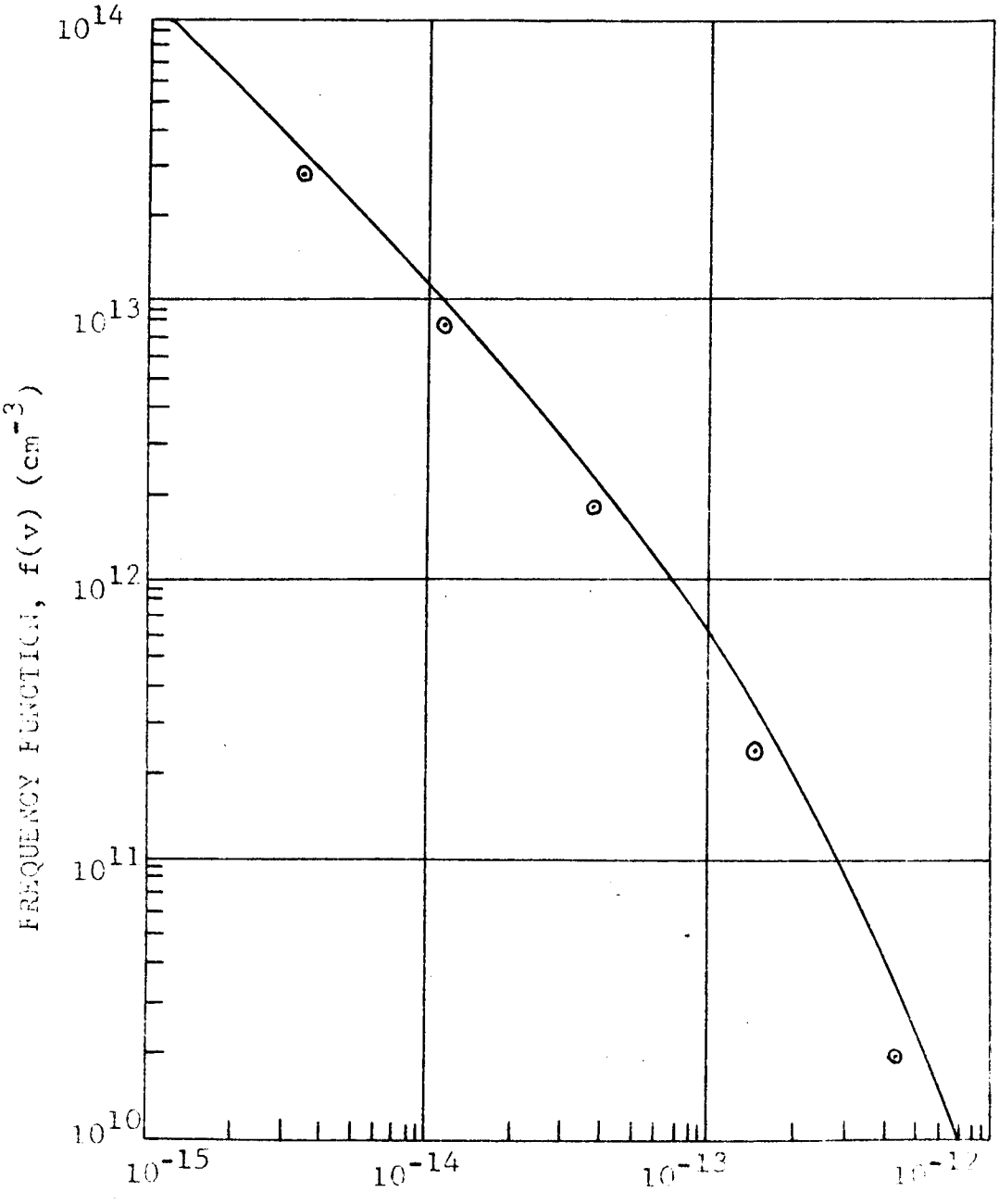

Figure-21 Theoretical Particle-Mass Distribution Function f(m) versus Particle Mass m.

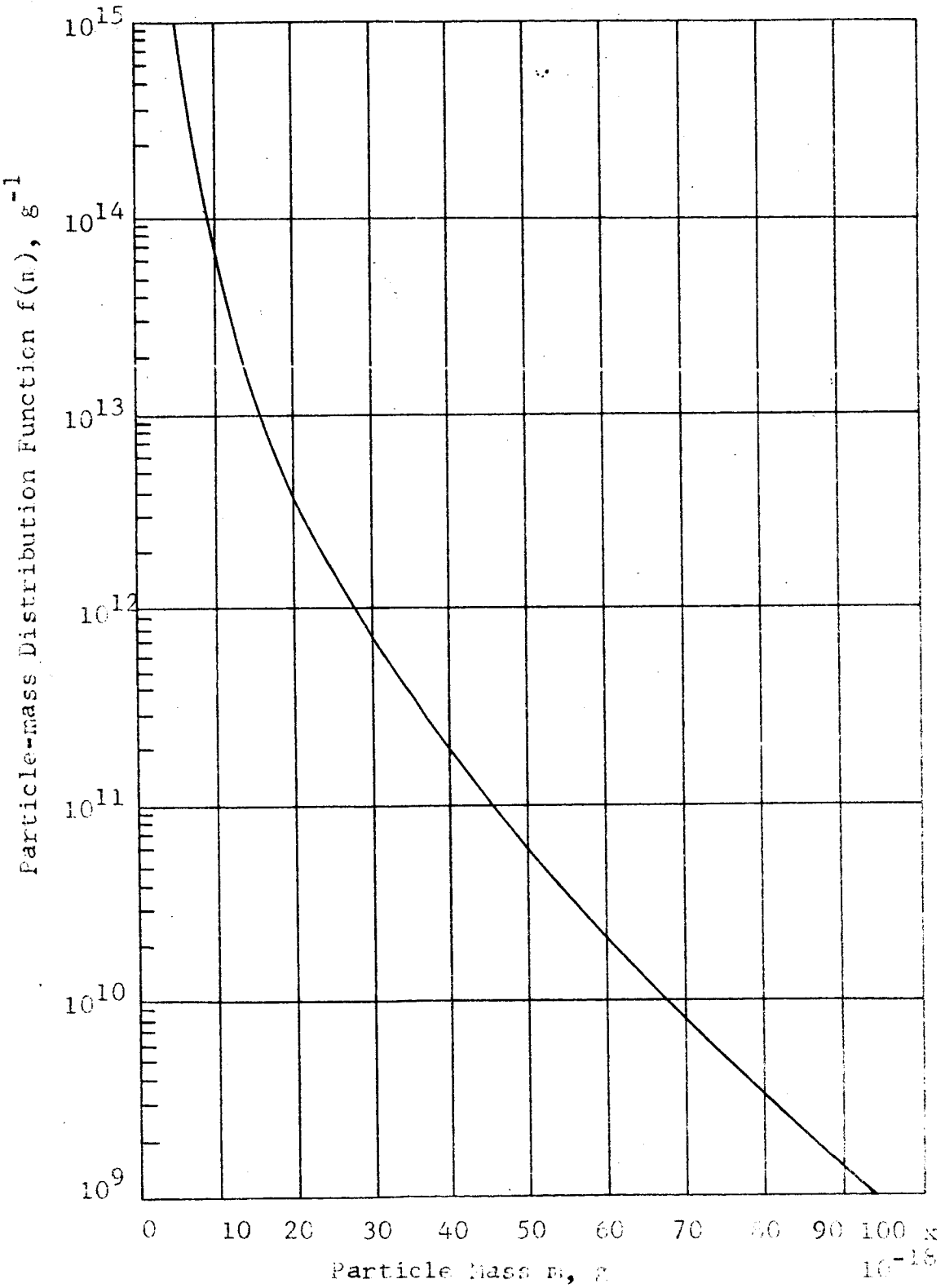

Figure-22 $\sqrt{m}\ f(m)$ versus m

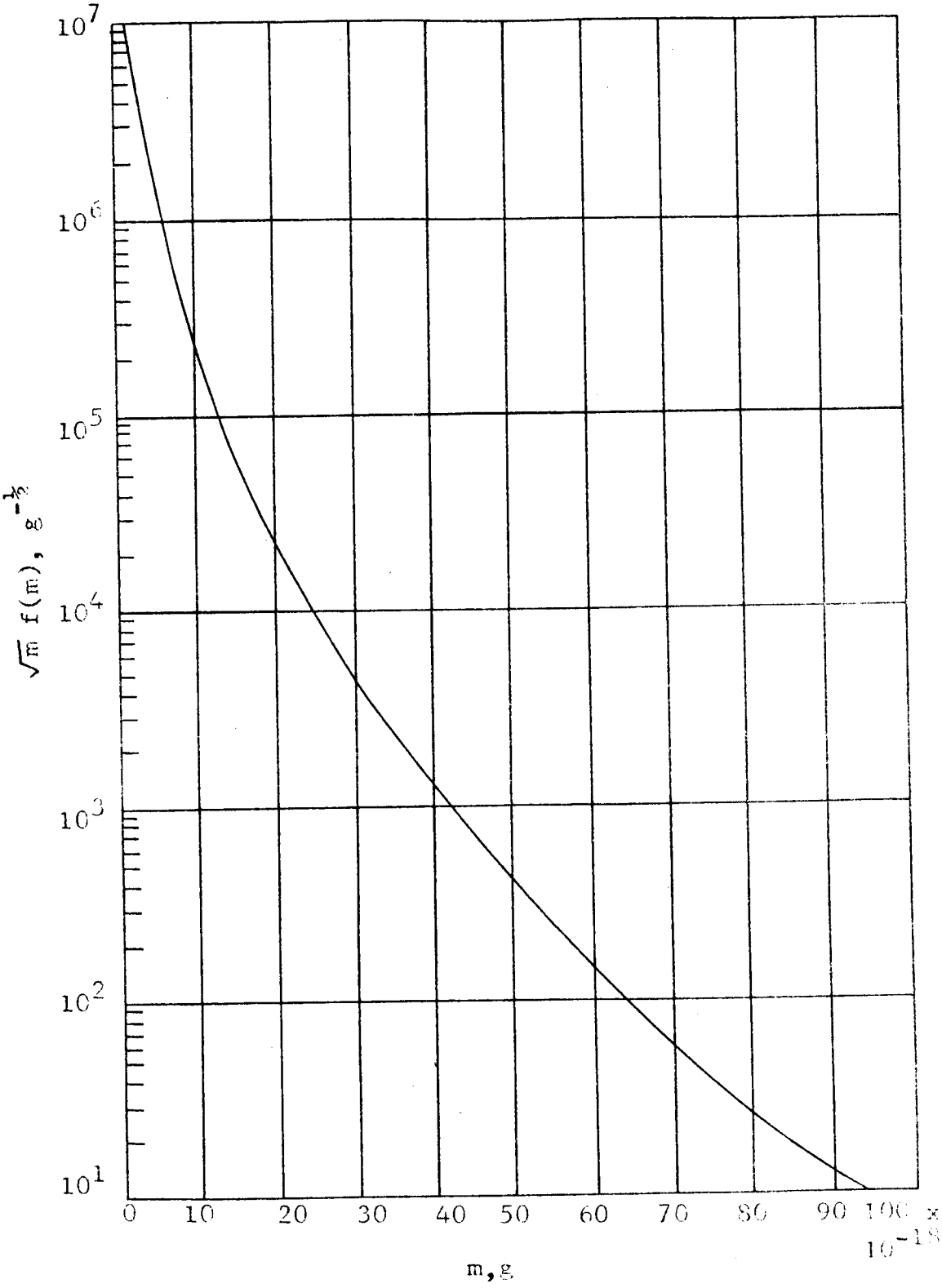

Figure-23 m f(m) versus m

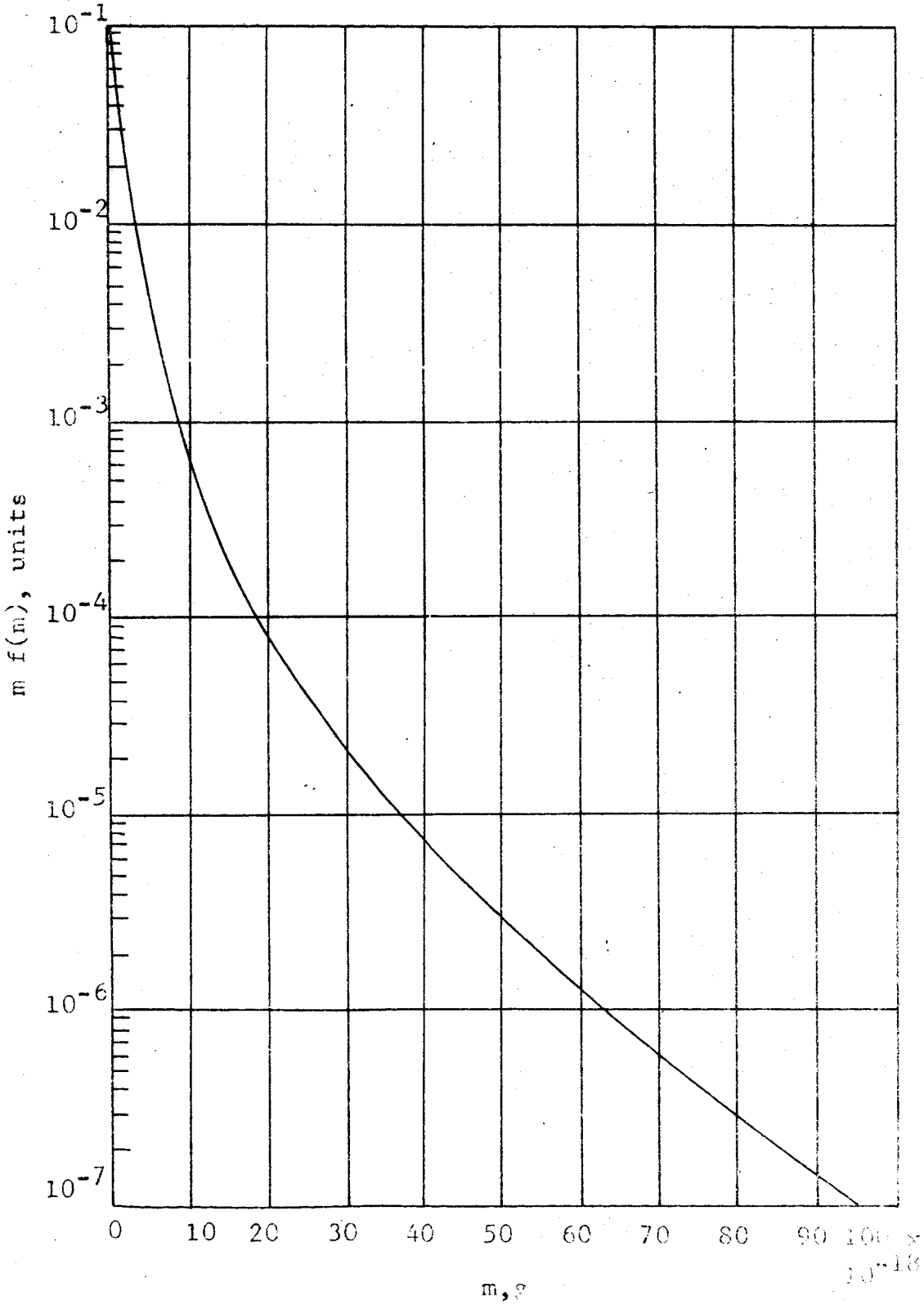

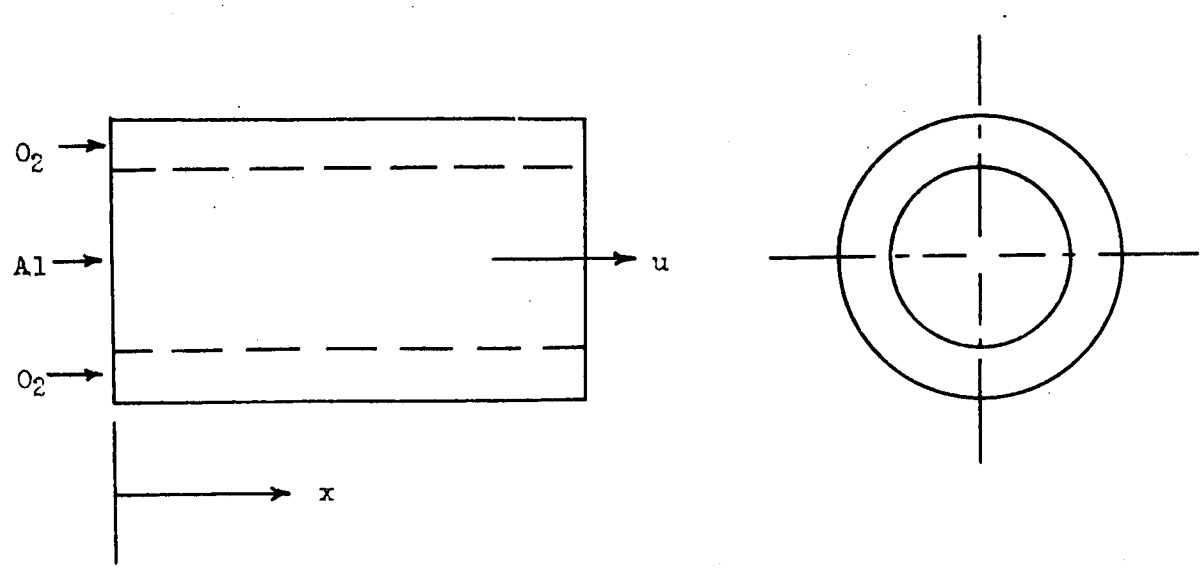

Figure-24 Schematic Diagram of a Vapor Phase Burning Model

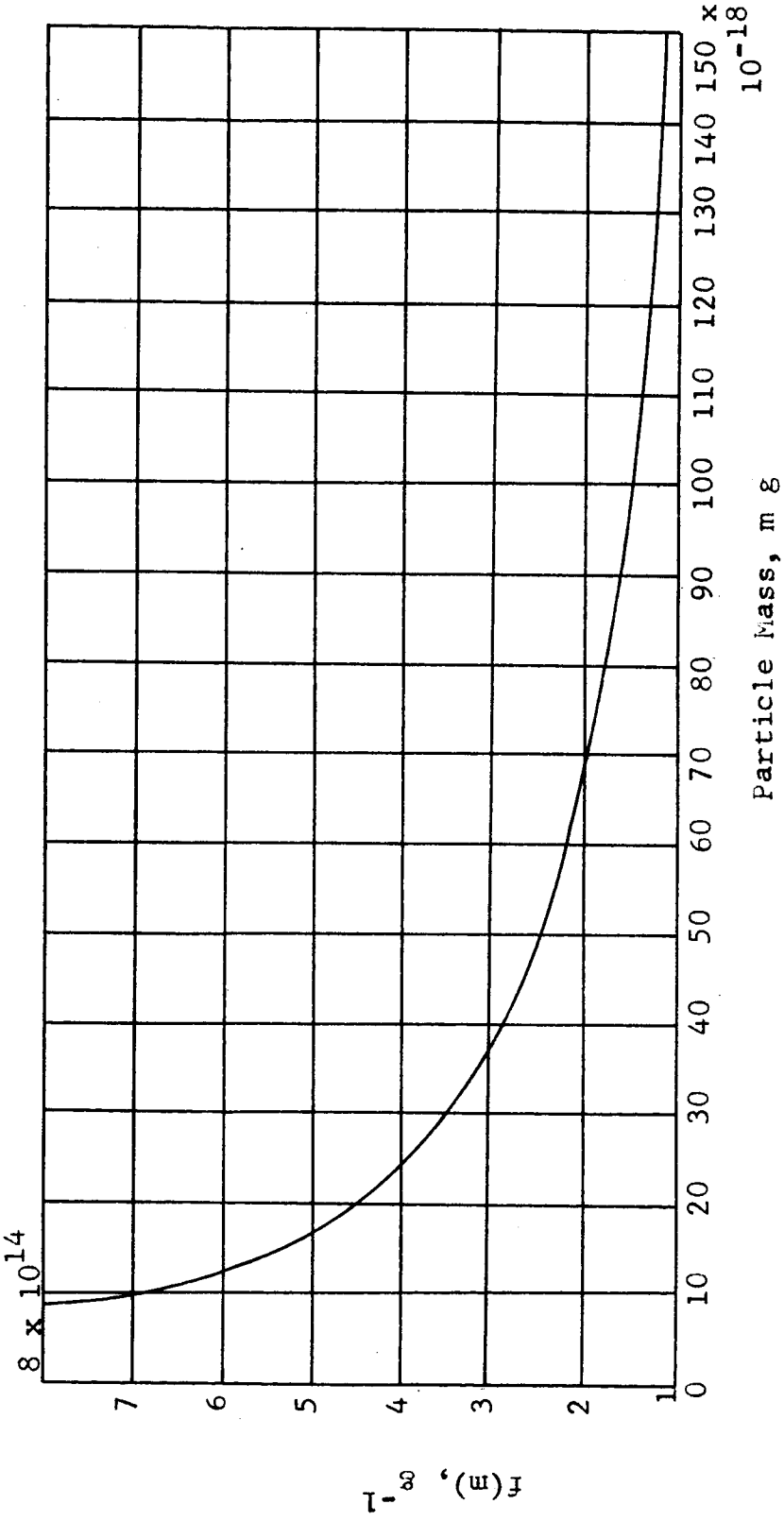

Figure-25 f(m) versus m

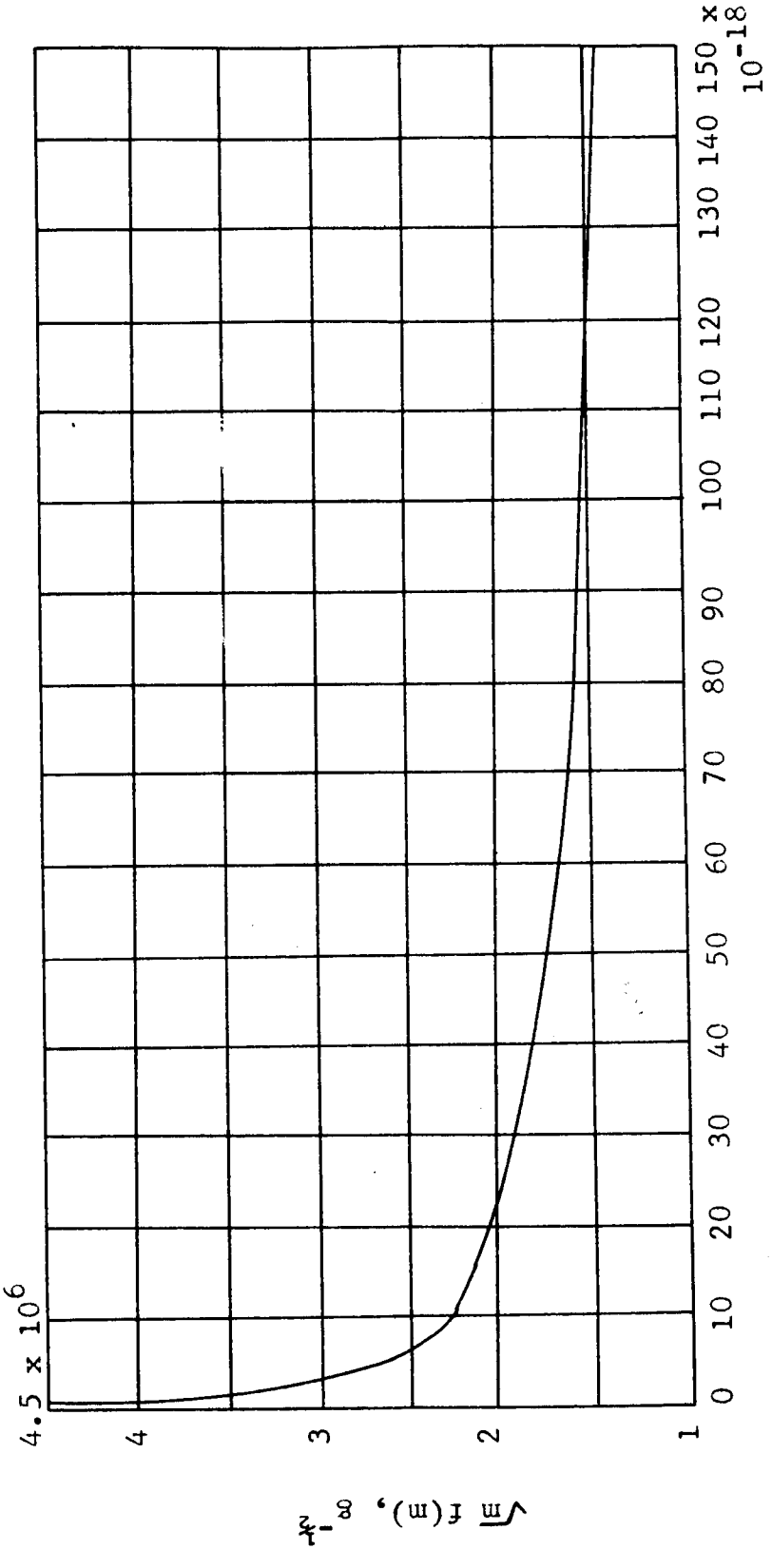

Figure-26 $\sqrt{m}$ f(m) versus m

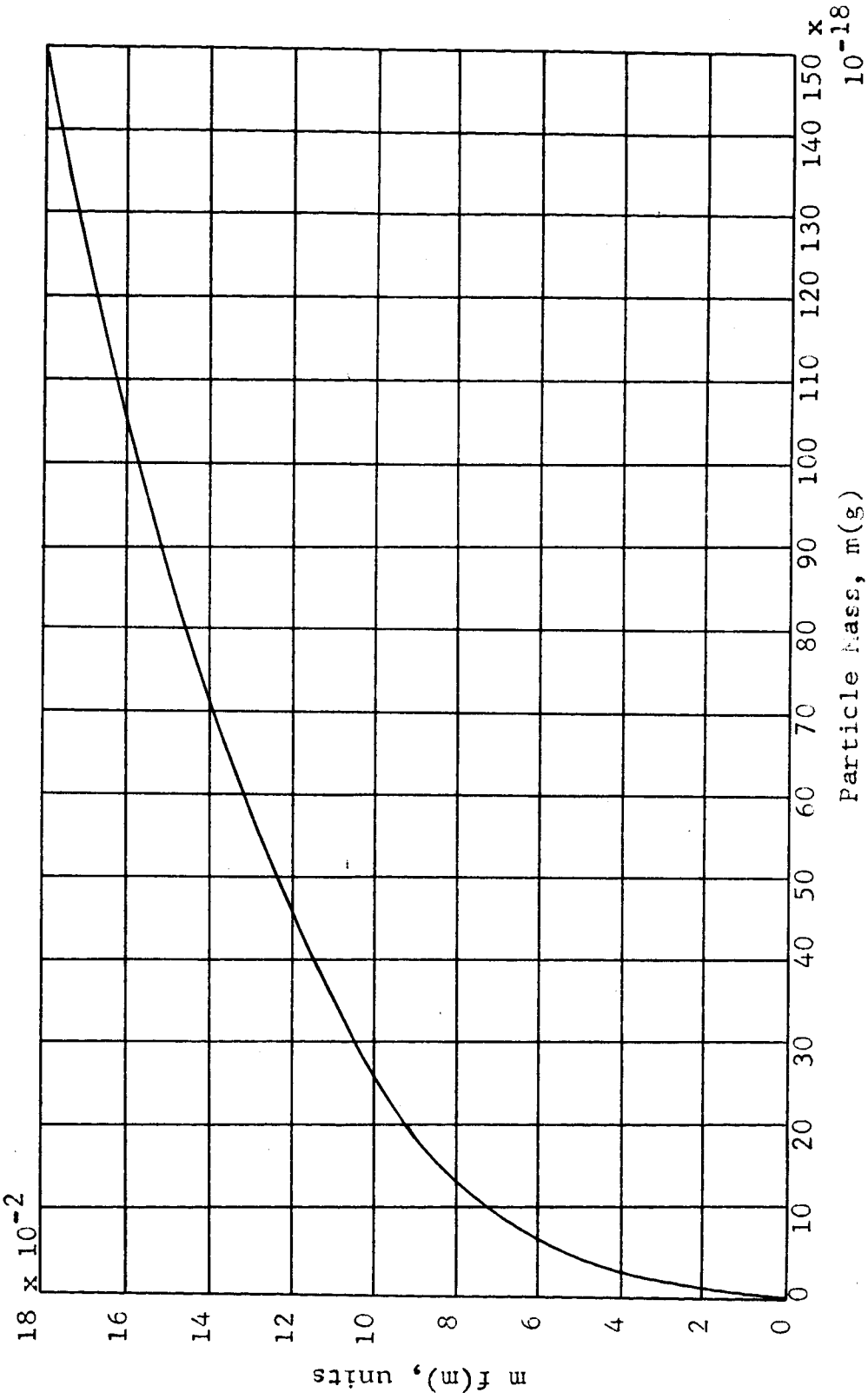

Figure-27 m f(m) versus m

TABLE I

BOILING AND MELTING POINTS OF METALS AND THEIR OXIDES

METAL	METAL M.P.°K	METAL B.P.°K	OXIDE	OXIDE M.P.°K	OXIDE B.P.°K	$\frac{V_{OXIDE}}{V_{METAL}}$	
Li	454	1620	Li_2O	1700	3200	0.58(4)	GROUP I
Na	371	1156	Na_2O	1190	1550	0.55(4)	
K	337(7)	1052(7)	K_2O	800(4)	1750(4)	0.45(4)	
Mg	923	1381	MgO	3075(4)	3350(4)	0.81(4)	
Ca	1123(7)	1693(7)	CaO	2873(7)	3800(7)	0.64(4)	
Al	932	2740	Al_2O_3	2318	3800(4)	1.45(4)	Group II
Be	1556	2750	BeO	2825	4123	1.68(4)	
Si	1685	3582	SiO_2	1883	3000		
Ti	1950	3550	TiO_2	2128	4100	1.73(4)	GROUP III
Zr	2125	4650	ZrO_2	2960	5200	1.45(4)	
B	2300	3950	B_2O_3	723	2520(4)		GROUP IV

* The numbers in brackets are the references from which the data were taken. Unmarked values came from reference 6.

GROUP I --- VOLATILE METAL
GROUP II--- NONVOLATILE METAL WITH INSOLUBLE OXIDE
GROUP III --- NONVOLATILE METAL WITH SOLUBLE OXIDE
GROUP IV --- NONVOLATILE METAL WITH VOLATILE OXIDE

TABLE II

ADIABATIC FLAME TEMPERATURE OF SOME METALS

$$X\,M(s) + Y/2\,O_2(g)$$

METAL	X	Y	T°K	COMBUSTION PRODUCTS, MOLE FRACTION
Al	2	3	3908	Al=0.064, AlO=0.094, Al_2O=0.209, O=0.366 O_2=0.097, Al_2O_3=0.172*
Mg	1	1	3229	Mg=0.171, MgO=0.484, O=0.053, O_2=0.059, MgO=0.233*
Li	2	1	2846	Li=0.370, LiO=0.041, Li_2O=0.164, O=0.015, O_2=0.075, Li_2O=0.334*
Be	1	1	4210	Be=0.218, BeO=0.033, $(BeO)_2$=0.012, $(BeO)_3$=0.012, O=0.189, O_2=0.014, BeO=0.522*
B	2	3	3786	B_2O_3=0.264, BO=0.500, B_2O_2=0.011, O=0.189, O_2=0.035

*marks denote the condensed phase; all other products are gaseous

TABLE III

IGNITION TEMPERATURES OF METALS IN $O_2(g)$

METAL	M.P., °C	IGNITION TEMPERATURE, °C
Li	179	190
Na	97.8	118
K	63	69
Mg	650	625
Ca	850	550
B	2100	——
Al	660	>1000
Ti	1730	——
Zr	1845	——

TABLE IV

The Compositions and Heat Balance in Al-O_2 Flame at Various Assumed Temperatures

Temperature, ^oK	3960	3970	3980	3990	4000
$Log_{10}K_P$	-2.4	-2.3	-2.2	-2.1	-2.0
β	0.382	0.432	0.5	0.582	0.683
Composition, Mole					
$Al_2O_3(l)$	0.618	0.568	0.5	0.418	0.317
Al(g)	0.382	0.432	0.5	0.582	0.683
AlO(g)	0.382	0.432	0.5	0.582	0.683
O(g)	0.764	0.864	1.0	1.164	1.366
Heat Contents of Products, Kcal	127.98	125.6	121.81	117.3	112.2
Dissociation Energy of $Al_2O_3(l)$, Kcal	214.0	243.0	281.3	327.0	384.0
Total Heat Consumption, Kcal	341.98	368.6	403.11	444.3	496.0
Heat of Formation of $Al_2O_3(l)$ at 298^oK, Kcal/mole	400.4	400.4	400.4	400.4	400.4

TABLE V

THERMODYNAMIC DATA FOR AL-O_2 SYSTEM

Al(gas); molecular weight, 26.98

T, °K	C_p°, cal/mole °K	$H_T^\circ - H_0^\circ$, cal/mole	S_T°, cal/mole °K	$-(F_T^\circ - H_0^\circ)$, cal/mole	H_T°, cal/mole	Formation from assigned reference elements	
						$(\Delta H_f^\circ)_T$, cal/mole	$\log_{10} K_f$
0	------	0	-------	0	75760.4	76857.6	-------
100	6.0209	588.2	33.3444	2746.3	76354.6	77331.1	-162.0725
200	5.2899	1144.8	37.2314	6301.5	76911.2	77454.1	-77.4971
298.15	5.1125	1653.6	39.5038	10064.8	77420.0	77420.0	-49.6588
300	5.1107	1663.1	39.5354	10137.5	77429.5	77418.7	-49.2889
400	5.0472	2170.5	40.7956	14147.7	77936.9	77328.6	-35.1966
500	5.0181	2673.6	41.9184	18285.6	78440.0	77204.5	-26.7528
600	5.0024	3174.6	42.8318	22524.5	78940.9	77048.6	-21.1340
700	4.9931	3674.3	43.6021	26847.2	79440.7	76862.0	-17.1293
800	4.9872	4173.3	44.2685	31241.5	79939.7	76645.0	-14.1338
900	4.9831	4671.8	44.8556	35698.2	80438.2	76397.9	-11.8109
1000	4.9802	5170.0	45.3805	40210.5	80936.3	73605.1	-9.9994
1100	4.9781	5667.9	45.8550	44772.7	81434.2	73403.0	-8.5392
1200	4.9765	6165.6	46.2881	49380.1	81932.0	73200.8	-7.3256
1300	4.9752	6663.2	46.6864	54029.1	82429.5	72998.3	-6.3014
1400	4.9742	7160.6	47.0550	58716.4	82927.0	72795.8	-5.4261
1500	4.9734	7658.0	47.3982	63439.3	83424.4	72593.2	-4.6696
1600	4.9728	8155.3	47.7192	68195.3	83921.7	72390.5	-4.0093
1700	4.9722	8652.6	48.0206	72982.5	84418.9	72187.7	-3.4286
1800	4.9718	9149.8	48.3048	77798.9	84916.2	71984.9	-2.9137
1900	4.9714	9646.9	48.5736	82642.9	85413.3	71782.1	-2.4543
2000	4.9711	10144.1	48.8286	87513.1	85910.4	71579.2	-2.0420
2100	4.9708	10641.2	49.0711	92408.2	86407.5	71376.3	-1.6702
2200	4.9706	11138.2	49.3024	97327.0	86904.6	71173.4	-1.3331
2300	4.9704	11635.3	49.5233	102268.3	87401.7	70970.5	-1.0261
2400	4.9703	12132.3	49.7348	107231.3	87898.7	70767.5	-0.7456
2500	4.9702	12629.3	49.9377	112215.0	88395.7	70564.5	-0.4882
2600	4.9701	13126.3	50.1327	117218.6	88892.7	70361.5	-0.2512
2700	4.9702	13623.4	50.3203	122241.3	89389.7	70158.5	-0.0324
2800	4.9703	14120.4	50.5010	127282.4	89886.8	69955.6	0.1700
2900	4.9705	14617.4	50.6754	132341.3	90383.8	69752.6	0.3581
3000	4.9709	15114.5	50.8439	137417.3	90880.9	69549.7	0.5330
3100	4.9715	15611.6	51.0069	142509.9	91378.0	69346.8	0.6963
3200	4.9723	16108.8	51.1648	147618.5	91875.2	69144.0	0.8489
3300	4.9735	16606.1	51.3178	152742.7	92372.5	68941.3	0.9916
3400	4.9750	17103.5	51.4663	157882.0	92869.9	68738.7	1.1257
3500	4.9769	17601.1	51.6105	163035.8	93367.5	68536.3	1.2517
3600	4.9794	18098.9	51.7508	168203.9	93865.3	68334.1	1.3705
3700	4.9824	18597.0	51.8873	173385.9	94363.4	68132.2	1.4824
3800	4.9862	19095.4	52.0202	178581.3	94861.8	67930.6	1.5883
3900	4.9908	19594.3	52.1498	183789.8	95360.6	67729.4	1.6883
4000	4.9964	20093.6	52.2762	189011.1	95860.0	67528.8	1.7831
4100	5.0030	20593.6	52.3995	194244.9	96359.9	67328.7	1.8729
4200	5.0107	21094.2	52.5203	199490.9	96860.6	67129.4	1.9581
4300	5.0188	21595.5	52.6382	204748.9	97361.8	66930.6	2.0392
4400	5.0291	22097.8	52.7537	210018.5	97864.2	66735.0	2.1164
4500	5.0403	22601.2	52.8668	215299.5	98367.5	66536.4	2.1900
4600	5.0535	23105.8	52.9777	220591.8	98872.2	66341.0	2.2601
4700	5.0685	23611.9	53.0866	225895.0	99378.3	66147.1	2.3272
4800	5.0854	24119.6	53.1935	231209.0	99886.0	65954.8	2.3910
4900	5.1035	24628.8	53.2985	236533.6	100395.2	65764.0	2.4525
5000	5.1243	25140.2	53.4018	241868.6	100906.6	65575.4	2.5110
5100	5.1473	25653.8	53.5035	247213.9	101420.2	65389.0	2.5670
5200	5.1727	26169.8	53.6037	252569.3	101936.1	65204.9	2.6208
5300	5.2004	26688.4	53.7025	257934.6	102454.8	65023.6	2.6725
5400	5.2307	27209.9	53.7999	263309.7	102976.3	64845.1	2.7220
5500	5.2636	27734.6	53.8962	268694.6	103501.0	64669.8	2.7696
5600	5.2992	28262.7	53.9914	274088.9	104029.1	64497.9	2.8154
5700	5.3376	28794.5	54.0855	279492.8	104560.9	64329.7	2.8595
5800	5.3774	29329.6	54.1785	284905.9	105096.0	64164.8	2.9021
5900	5.4214	29869.5	54.2708	290328.4	105635.9	64004.7	2.9430
6000	5.4402	30398.0	54.3594	295758.6	106164.4	63853.2	2.9823

AlO(gas); molecular weight, 42.98

T, °K	C_p°, cal/mole °K	$H_T^\circ - H_0^\circ$, cal/mole	S_T°, cal/mole °K	$-(F_T^\circ - H_0^\circ)$, cal/mole	H_f°, cal/mole	Formation from assigned reference elements	
						$(\Delta H_f^\circ)_f$, cal/mole	$\log_{10} K_f$
0	------	0	-------	0	18715.5	20844.1	-------
100	6.9573	695.0	44.4610	3751.1	19410.5	21077.6	-41.2307
200	7.0519	1393.5	49.2990	8466.3	20109.0	20994.6	-18.2172
298.15	7.3815	2100.5	52.1709	13454.2	20816.0	20816.0	-10.6920
300	7.3887	2114.2	52.2166	13550.8	20829.7	20812.4	-10.5979
400	7.7654	2872.3	54.3950	18885.7	21587.8	20617.9	-6.8237
500	8.0667	3664.6	56.1617	24416.2	22380.2	20417.5	-4.5807
600	8.2879	4482.9	57.6531	30108.9	23198.5	20201.4	-3.1007
700	8.4488	5320.2	58.9434	35940.2	24035.7	19963.3	-2.0553
800	8.5677	6171.3	60.0798	41892.5	24886.8	19699.6	-1.2611
900	8.6578	7032.8	61.0943	47952.1	25748.3	19408.4	-0.6874
1000	8.7277	7902.2	62.0103	54108.1	26617.7	16573.1	-0.2602
1100	8.7835	8777.9	62.8448	60351.4	27493.4	16329.3	0.0666
1200	8.8289	9658.6	63.6111	66674.8	28374.1	16085.8	0.3350
1300	8.8668	10543.4	64.3193	73071.7	29258.9	15842.2	0.5587
1400	8.8989	11431.7	64.9776	79537.0	30147.2	15598.6	0.7475
1500	8.9268	12323.0	65.5926	86065.8	31038.6	15354.5	0.9086
1600	8.9512	13217.0	66.1695	92654.2	31932.5	15110.0	1.0474
1700	8.9731	14113.2	66.7128	99298.6	32828.7	14864.8	1.1677
1800	8.9928	15011.5	67.2263	105995.8	33727.0	14618.7	1.2731
1900	9.0108	15911.7	67.7130	112743.0	34627.2	14371.7	1.3658
2000	9.0276	16813.6	68.1756	119537.6	35529.2	14123.7	1.4478
2100	9.0432	17717.2	68.6164	126377.4	36432.7	13874.4	1.5205
2200	9.0580	18622.2	69.0375	133260.2	37337.8	13623.9	1.5855
2300	9.0722	19528.8	69.4404	140184.2	38244.3	13372.2	1.6438
2400	9.0858	20436.7	69.8268	147147.7	39152.2	13119.0	1.6963
2500	9.0991	21345.9	70.1980	154149.1	40061.4	12864.6	1.7435
2600	9.1123	22256.5	70.5551	161186.9	40972.0	12608.8	1.7865
2700	9.1253	23168.4	70.8993	168259.7	41883.9	12351.8	1.8254
2800	9.1384	24081.5	71.2314	175366.3	42797.1	12093.5	1.8606
2900	9.1517	24996.0	71.5523	182505.6	43711.6	11834.1	1.8930
3000	9.1652	25911.9	71.8628	189676.4	44627.4	11573.5	1.9222
3100	9.1790	26829.1	72.1635	196877.8	45544.6	11312.1	1.9492
3200	9.1934	27747.7	72.4552	204108.8	46463.2	11049.7	1.9739
3300	9.2082	28667.8	72.7383	211368.6	47383.3	10786.6	1.9964
3400	9.2237	29589.4	73.0134	218656.2	48304.9	10522.9	2.0171
3500	9.2399	30512.5	73.2810	225971.0	49228.1	10258.8	2.0362
3600	9.2568	31437.4	73.5415	233312.2	50152.9	9994.4	2.0538
3700	9.2745	32363.9	73.7954	240679.1	51079.5	9729.8	2.0699
3800	9.2930	33292.3	74.0430	248071.1	52007.8	9465.2	2.0850
3900	9.3124	34222.6	74.2846	255487.5	52938.1	9200.7	2.0987
4000	9.3328	35154.8	74.5207	262927.8	53870.3	8936.6	2.1115
4100	9.3542	36089.2	74.7514	270391.5	54804.7	8673.0	2.1232
4200	9.3765	37025.7	74.9770	277877.9	55741.2	8410.1	2.1340
4300	9.3998	37964.5	75.1980	285386.7	56680.0	8147.9	2.1439
4400	9.4242	38905.7	75.4143	292917.4	57621.2	7886.8	2.1532
4500	9.4496	39849.4	75.6264	300469.4	58564.9	7626.7	2.1618
4600	9.4761	40795.6	75.8344	308042.5	59511.2	7368.0	2.1697
4700	9.5036	41744.6	76.0385	315636.2	60460.1	7110.7	2.1771
4800	9.5321	42696.4	76.2388	323250.1	61411.9	6855.1	2.1838
4900	9.5618	43651.1	76.4357	330883.8	62366.6	6601.1	2.1901
5000	9.5924	44608.8	76.6292	338537.1	63324.3	6349.1	2.1959
5100	9.6241	45569.6	76.8194	346209.6	64285.1	6099.1	2.2012
5200	9.6568	46533.6	77.0066	353900.9	65249.1	5851.3	2.2061
5300	9.6904	47501.0	77.1909	361610.8	66216.5	5605.8	2.2107
5400	9.7251	48471.7	77.3724	369339.0	67187.3	5362.7	2.2149
5500	9.7607	49446.0	77.5511	377085.2	68161.6	5122.2	2.2186
5600	9.7972	50423.9	77.7273	384849.1	69139.4	4884.3	2.2222
5700	9.8346	51405.5	77.9011	392630.6	70121.0	4649.3	2.2254
5800	9.8729	52390.9	78.0724	400429.2	71106.4	4417.1	2.2286
5900	9.9121	53380.1	78.2415	408245.0	72095.6	4188.0	2.2313
6000	9.9520	54373.3	78.4085	416077.5	73088.8	3962.0	2.2337

Al_2O_3 (crystal, liquid); molecular weight, 101.96

T, °K	C_p°, cal/mole °K	$H_T^\circ - H_0^\circ$,[a] cal/mole	S_T°, cal/mole °K	$-(F_T^\circ - H_0^\circ)/T$,[a] cal/mole	H_T°, cal/mole	Formation from assigned reference elements	
						$(\Delta H_f^\circ)_f$, cal/mole	$\log_{10} K_f$
0	------	0	0	0	-402794.4	-397499.9	-------
100	3.0688	78.0	1.0241	24.5	-402716.4	-398691.6	897.2300
200	12.2228	841.5	5.9465	347.8	-401952.9	-399839.0	421.3514
298.15	18.8840	2396.4	12.1750	1235.6	-400400.0	-400400.0	277.1216
300	18.9794	2429.3	12.2897	1257.6	-400365.1	-400406.2	275.3114
400	22.9876	4545.2	18.3509	2735.2	-398249.2	-400550.6	202.3746
500	25.3442	6970.8	23.7524	4905.4	-395823.6	-400476.0	158.6089
600	26.8881	9587.5	28.5206	7524.9	-393206.9	-400305.8	129.4413
700	27.9685	12333.2	32.7510	10592.5	-390461.2	-400099.9	108.6174
800	28.7572	15171.4	36.5392	14060.0	-387623.0	-399840.2	93.0072
900	29.3523	18078.4	39.9618	17887.2	-384716.0	-399695.4	80.8722
b1000	29.8136	21037.5	43.0784	22040.9	-381756.9	-404559.6	71.0878
1100	30.1745	24036.8	45.9393	26496.4	-378757.6	-404218.7	63.0538
1200	30.4617	27069.8	48.5779	31223.7	-375724.6	-403858.4	56.3644
1300	30.9068	30141.0	51.0360	36205.8	-372653.4	-403472.2	50.7095
1400	31.2819	33250.6	53.3402	41425.8	-369543.8	-403058.7	45.8670
1500	31.6436	36396.9	55.5109	46869.4	-366397.5	-402618.4	41.6747
1600	31.9951	39578.9	57.5644	52524.1	-363215.5	-402151.7	38.0109
1700	32.3389	42795.7	59.5144	58378.8	-359998.7	-401659.3	34.7815
1800	32.6766	46046.5	61.3724	64423.9	-356747.9	-401141.5	31.9148
1900	33.0094	49330.8	63.1481	70650.5	-353463.5	-400598.8	29.3533
2000	33.3382	52648.3	64.8496	77051.0	-350146.1	-400031.4	27.0511
2100	33.6639	55998.4	66.4841	83618.2	-346796.0	-399439.6	24.9709
2200	33.9870	59381.0	68.0576	90345.8	-343413.4	-398823.7	23.0827
2300	34.3079	62795.7	69.5755	97227.9	-339998.7	-398183.9	21.3616
c2318	34.365	63413.8	69.843	98482.3	-339380.6	-398063.3	21.0672
2318	35.0	89413.8	81.060	98482.3	-313380.6	-372051.2	21.0672
2400	35.0	92283.8	82.2765	105179.8	-310510.6	-371478.8	19.9703
2500	35.0	95783.8	83.7053	113479.4	-307010.6	-370769.9	18.5184
2600	35.0	99283.8	85.078C	121919.0	-303510.6	-370068.9	17.2732
2700	35.0	102783.8	86.3989	130493.3	-300010.6✓	-369375.7	16.1223
2800	35.0	106283.8	87.6718	139197.2	-296510.6	-368690.1	15.0553
2900	35.0	109783.8	88.9000	148026.2	-293010.6	-368012.0	14.0642
3000	35.0	113283.8	90.0865	156975.8	-289510.6	-367341.0	13.1434
3100	35.0	116783.8	91.2342	166042.2	-286010.6	-366677.1	12.2781
3200	35.0	120283.8	92.3454	175221.4	-282510.6	-366020.0	11.4712
3300	35.0	123783.8	93.4224	184510.1	-279010.5	-365369.5	10.7141
3400	35.0	127283.8	94.4672	193904.8	-275510.6	-364725.3	10.0031
3500	35.0	130783.8	95.4818	203402.5	-272010.6	-364087.3	9.3338
3600	35.0	134283.8	96.4678	213000.2	-268510.6	-363455.1	8.7029
3700	35.0	137783.8	97.4267	222695.2	-265010.6	-362828.5	8.1070
3800	35.0	141283.8	98.3601 ✓	232484.7	-261510.6	-362207.4 ✓	7.5439
3900	35.0	144783.8	99.2693	242366.4	-258010.6	-361591.5	7.0101
4000	35.0	148283.8	100.1554	252337.8	-254510.6	-360980.6	6.5041
4100	35.0	151783.8	101.0196	262396.7	-251010.6	-360374.4	6.0234
4200	35.0	155283.8	101.8631	272541.1	-247510.6	-359772.9	5.5663
4300	35.0	158783.8	102.6866	282768.7	-244010.6	-359175.7	5.1312
4400	35.0	162283.8	103.4912	293077.7	-240510.6	-358582.8	4.7156
4500	35.0	165783.8	104.2778	303466.3	-237010.6	-357993.9	4.3213
4600	35.0	169283.8	105.0471	313932.7	-233510.6	-357408.9	3.9436
4700	35.0	172783.8	105.7998	324475.2	-230010.6	-356827.7	3.5828
4800	35.0	176283.8	106.5367	335092.2	-226510.6	-356250.0	3.2372
4900	35.0	179783.8	107.2583	345782.0	-223010.6	-355675.8	2.9066
5000	35.0	183283.8	107.9654	356543.3	-219510.6	-355105.0	2.5897
5100	35.0	186783.8	108.6585	367374.6	-216010.6	-354537.5	2.2855
5200	35.0	190283.8	109.3381	378274.6	-212510.6	-353973.0	1.9935
5300	35.0	193783.8	110.0048	389241.8	-209010.6	-353411.7	1.7132
5400	35.0	197283.8	110.6591	400275.1	-205510.6	-352853.2	1.4435
5500	35.0	200783.8	111.3013	411373.3	-202010.6	-352297.6	1.1838
5600	35.0	204283.8	111.9319	422535.0	-198510.6	-351744.8	0.9341
5700	35.0	207783.8	112.5514	433759.3	-195010.6	-351194.7	0.6934
5800	35.0	211283.8	113.1601	445045.0	-191510.6	-350647.2	0.4618
5900	35.0	214783.8	113.7584	456391.0	-188010.6	-350102.3	0.2379
6000	35.0	218283.8	114.3467	467796.3	-184510.6	-349559.9	0.0217

O(gas); molecular weight, 16.0

T, °K	C_p°, cal/mole °K	$H_T^\circ - H_0^\circ$, cal/mole	S_T°, cal/mole °K	$-(F_T^\circ - H_0^\circ)/T$, cal/mole	H_f°, cal/mole	Formation from assigned reference elements	
						$(\Delta H_f^\circ)_f$, cal/mole	$\log_{10} K_f$
0	------	0	-------	0	59949.1	58986.5	--------
100	5.5656	527.5	32.4662	2719.1	58476.6	59167.2	-126.7319
200	5.4341	1084.9	36.3400	6183.1	59034.0	59376.7	-61.9894
298.15	5.2375	1607.2	38.4688	9861.9	59556.6	59556.6	-40.6022
300	5.2347	1617.2	38.5033	9933.1	59566.3	59559.8	-40.3330
400	5.1347	2135.1	39.9317	13861.6	60084.3	59722.7	-29.4725
500	5.0808	2645.6	41.1311	17919.9	60594.8	59867.6	-22.9391
600	5.0490	3152.0	42.0544	22040.6	61101.1	59990.4	-18.5735
700	5.0287	3655.8	42.8311	26325.9	61605.0	60111.2	-15.4488
800	5.0154	4158.0	43.5016	30643.3	62107.1	60214.6	-13.1010
900	5.0059	4659.0	44.0918	35023.6	62608.2	60308.6	-11.2719
1000	4.9990	5159.3	44.6188	39459.6	63108.4	60395.0	-9.8065
1100	4.9938	5658.9	45.0950	43945.7	63608.0	60475.1	-8.6058
1200	4.9898	6158.1	45.5294	48477.2	64107.2	60550.1	-7.6040
1300	4.9867	6656.9	45.9280	53050.4	64606.0	60620.5	-6.7552
1400	4.9842	7155.4	46.2981	57661.9	65104.6	60687.1	-6.0269
1500	4.9823	7653.7	46.6419	62309.1	65602.9	60750.1	-5.3951
1600	4.9807	8151.9	46.9634	66989.6	66101.0	60809.7	-4.8416
1700	4.9795	8649.9	47.2653	71701.2	66599.0	60866.3	-4.3528
1800	4.9786	9147.8	47.5497	76442.1	67096.9	60919.8	-3.9179
1900	4.9780	9645.6	47.8191	81210.6	67594.8	60970.5	-3.5285
2000	4.9778	10143.4	48.0744	86005.4	68092.5	61018.3	-3.1777
2100	4.9780	10641.2	48.3173	90825.1	68590.3	61063.3	-2.8601
2200	4.9786	11139.0	48.5487	95668.5	69088.2	61105.5	-2.5712
2300	4.9797	11636.9	48.7702	100534.5	69586.1	61145.1	-2.3072
2400	4.9814	12135.0	48.9822	105422.2	70084.1	61182.2	-2.0650
2500	4.9836	12633.2	49.1856	110330.7	70582.4	61216.7	-1.8421
2600	4.9864	13131.7	49.3811	115259.1	71080.9	61248.9	-1.6362
2700	4.9899	13630.5	49.5693	120206.6	71579.7	61278.8	-1.4455
2800	4.9940	14129.7	49.7509	125172.7	72078.9	61306.5	-1.2683
2900	4.9988	14629.4	49.9262	130156.6	72578.5	61332.2	-1.1033
3000	5.0043	15129.5	50.0956	135157.8	73078.6	61356.0	-0.9492
3100	5.0104	15630.2	50.2594	140175.6	73579.4	61378.0	-0.8050
3200	5.0172	16131.6	50.4181	145209.6	74080.8	61398.4	-0.6698
3300	5.0246	16633.7	50.5718	150259.3	74582.8	61417.3	-0.5427
3400	5.0327	17136.5	50.7211	155324.2	75085.7	61434.9	-0.4230
3500	5.0413	17640.2	50.8659	160403.9	75589.4	61451.3	-0.3102
3600	5.0504	18144.8	51.0114	165498.0	76094.0	61466.6	-0.2036
3700	5.0600	18650.3	51.1504	170606.1	76599.5	61481.0	-0.1027
3800	5.0701	19156.8	51.2859	175727.9	77106.0	61494.5	-0.0072
3900	5.0806	19664.4	51.4173	180863.1	77613.5	61507.4	0.0835
4000	5.0915	20173.0	51.5461	186011.3	78122.1	61519.6	0.1697
4100	5.1027	20682.7	51.6719	191172.2	78631.8	61531.4	0.2517
4200	5.1141	21193.5	51.7950	196345.6	79142.7	61542.7	0.3298
4300	5.1258	21705.5	51.9155	201531.1	79654.7	61553.8	0.4043
4400	5.1376	22218.7	52.0335	206728.6	80167.8	61564.6	0.4754
4500	5.1496	22733.0	52.1491	211937.8	80682.2	61575.2	0.5433
4600	5.1617	23248.6	52.2624	217158.3	81197.8	61585.8	0.6083
4700	5.1738	23765.4	52.3735	222390.2	81714.5	61596.3	0.6706
4800	5.1860	24283.4	52.4826	227633.0	82232.5	61606.9	0.7303
4900	5.1981	24802.6	52.5896	232886.6	82751.7	61617.5	0.7875
5000	5.2102	25323.0	52.6948	238150.8	83272.1	61628.1	0.8425
5100	5.2223	25844.6	52.7981	243425.5	83793.8	61638.9	0.8953
5200	5.2342	26367.4	52.8996	248710.4	84316.6	61649.9	0.9461
5300	5.2460	26891.5	52.9994	254005.4	84840.6	61661.1	0.9950
5400	5.2577	27416.5	53.0976	259310.2	85365.8	61672.4	1.0421
5500	5.2691	27943.0	53.1941	264624.8	85892.1	61683.9	1.0875
5600	5.2804	28470.5	53.2892	269949.0	86419.6	61695.7	1.1312
5700	5.2915	28999.1	53.3826	275282.6	86948.2	61707.7	1.1735
5800	5.3024	29528.8	53.4747	280625.3	87477.9	61719.9	1.2144
5900	5.3131	30059.5	53.5650	285977.5	88008.7	61732.3	1.2537
6000	5.3235	30591.4	53.6550	291338.6	88540.5	61744.9	1.2918